

1           NON-CROSSING NONLINEAR REGRESSION  
2 QUANTILES BY MONOTONE COMPOSITE QUANTILE  
3           REGRESSION NEURAL NETWORK, WITH  
4           APPLICATION TO RAINFALL EXTREMES

5                           Alex J. Cannon\*

Climate Research Division, Environment and Climate Change Canada,  
Victoria, British Columbia, Canada

---

\*Corresponding author: Email <alex.cannon@canada.ca>; Phone +1-250-363-8006

## Abstract

The goal of quantile regression is to estimate conditional quantiles for specified values of quantile probability using linear or nonlinear regression equations. These estimates are prone to “quantile crossing”, where regression predictions for different quantile probabilities do not increase as probability increases. In the context of the environmental sciences, this could, for example, lead to estimates of the magnitude of a 10-yr return period rainstorm that exceed the 20-yr storm, or similar nonphysical results. This problem, as well as the potential for overfitting, is exacerbated for small to moderate sample sizes and for nonlinear quantile regression models. As a remedy, this study introduces a novel nonlinear quantile regression model, the monotone composite quantile regression neural network (MCQRNN), that (1) simultaneously estimates multiple non-crossing, nonlinear conditional quantile functions; (2) allows for optional monotonicity, positivity/non-negativity, and generalized additive model constraints; and (3) can be adapted to estimate standard least-squares regression and non-crossing expectile regression functions. First, the MCQRNN model is evaluated on synthetic data from multiple functions and error distributions using Monte Carlo simulations. MCQRNN outperforms the benchmark models, especially for non-normal error distributions. Next, the MCQRNN model is applied to real-world climate data by estimating rainfall Intensity-Duration-Frequency (IDF) curves at locations in Canada. IDF curves summarize the relationship between the intensity and occurrence frequency of extreme rainfall over storm durations ranging from minutes to a day. Because annual maximum rainfall intensity is a non-negative quantity that should increase monotonically as the occurrence frequency and storm duration decrease, monotonicity and non-negativity constraints are key constraints in IDF curve estimation. In comparison to standard QRNN models, the ability of the MCQRNN model to incorporate these constraints, in addition to non-crossing, leads to more robust and realistic estimates of extreme rainfall.

# 1 Introduction

Estimating regression quantiles – conditional quantiles of a response variable that depend on covariates in some form of regression equation – is a fundamental task in data-driven science. Focusing on the environmental sciences, quantile regression methods have been used to provide estimates of predictive uncertainty in forecast applications (Cawley *et al.*, 2007); construct growth curves for organisms (Muggeo *et al.*, 2013); relate soil moisture deficit with summer hot extremes (Hirschi *et al.*, 2010); provide flood frequency estimates (Ouali *et al.*, 2016); estimate rainfall Intensity-Duration-Frequency (IDF) curves (Ouali and Cannon, 2017); determine the relation between rainfall intensity and duration and landslide occurrence (Saito *et al.*, 2010); estimate trends in climate, streamflow, and sea level data (Koenker and Schorfheide, 1994; Barbosa, 2008; Al-lamano *et al.*, 2009; Roth *et al.*, 2015); downscale atmospheric model outputs (Friederichs and Hense, 2007; Cannon, 2011; Ben Alaya *et al.*, 2016); and determine scaling relationships between temperature and extreme precipitation (Wasko and Sharma, 2014), among other applications.

Quantile regression equations can be linear or nonlinear. In most variants, including the original linear model (Koenker and Bassett Jr., 1978), conditional quantiles for specified quantile probabilities are estimated separately by different regression equations; together, these different equations can be used to build up a piecewise estimate of the conditional response distribution. However, given finite samples, this flexibility can lead to “quantile crossing” where, for some values of the covariates, quantile regression predictions do not increase with the specified quantile probability  $\tau$ . For instance, the  $\tau_1 = 0.1$ -quantile (10<sup>th</sup>-percentile) estimate may be greater in magnitude than the  $\tau_2 = 0.2$ -quantile (20<sup>th</sup>-percentile) estimate, which violates the property that the conditional quantile function be strictly monotonic. As Ouali *et al.* (2016) state, “crossing quantile regression is a serious modeling problem that may lead to an invalid response distribution”.

Three main approaches have been used to solve the quantile crossing problem: post-processing, stepwise estimation, and simultaneous estimation. In post-processing, non-crossing quantiles are enforced following model estimation by rearranging predictions so that they increase with increasing  $\tau$  (Chernozhukov *et al.*, 2010). In stepwise estimation, regression equations are constructed

57 iteratively, with constraints added so that each subsequent quantile regression function does not  
58 cross the one estimated previously (*Liu and Wu, 2009; Muggeo et al., 2013*). Finally, in simultane-  
59 ous estimation, quantile regression equations for all desired values of  $\tau$  are estimated at the same  
60 time, with additional constraints added to parameter optimization to ensure non-crossing (*Takeuchi*  
61 *et al., 2006; Bondell et al., 2010; Liu and Wu, 2011; Bang et al., 2016*). Unlike sequential esti-  
62 mation, simultaneous estimation is attractive because it does not depend on the order in which  
63 quantiles are estimated. Furthermore, fitting for multiple values of  $\tau$  simultaneously allows one  
64 to “borrow strength” across regression quantiles and improve overall model performance (*Bang*  
65 *et al., 2016*). This property is especially useful for nonlinear quantile regression models, which  
66 are more prone to overfitting and quantile crossing in the face of small to moderate sample sizes  
67 (*Muggeo et al., 2013*).

68 *Baldwin (2006)*, paraphrasing *Persson (2001)*, states “...while there is only one way to be linear,  
69 there are an uncountable infinity of ways to be nonlinear. One cannot check them all”. For a flexi-  
70 ble nonlinear model like a neural network, imposing extra constraints, for example as informed by  
71 process knowledge, can be useful for narrowing the overall search space of potential nonlinearities.  
72 As a simple example, growth curves should increase monotonically with the age of the organism,  
73 which led *Muggeo et al. (2013)* to introduce a monotonicity constraint in addition to the non-  
74 crossing constraint. Similarly, *Roth et al. (2015)* applied nonlinear monotone quantile regression  
75 to describe non-decreasing trends in rainfall extremes. *Takeuchi et al. (2006)* developed a nonpara-  
76 metric, kernelized version of quantile regression with similarities to support vector machines; both  
77 non-crossing and monotonicity constraints are considered, with directions on the incorporation of  
78 other constraints, such as positivity and additivity constraints, also provided. However, standard  
79 implementations of the kernel quantile regression model (e.g., *Karatzoglou et al., 2004; Hofmeis-*  
80 *ter, 2017*) are computationally costly, with complexity that is cubic in the number of samples, and  
81 do not explicitly implement the proposed constraints.

82 As an alternative, this study introduces an efficient, flexible nonlinear quantile regression  
83 model, the monotone composite quantile regression neural network (MCQRNN), that: (1) si-

84 multaneously estimates multiple non-crossing quantile functions; (2) allows for optional mono-  
85 tonicity, positivity/non-negativity, and additivity constraints, as well as fine-grained control on the  
86 degree of non-additivity; and (3) can be modified to estimate standard least-squares regression and  
87 non-crossing expectile regression functions. These features, which are combined into a single,  
88 unified framework, are made possible through a novel combination of elements drawn from the  
89 standard QRNN model (*White, 1992, Taylor, 2000 and Cannon, 2011*), the monotone multi-layer  
90 perceptron (MMLP) (*Zhang and Zhang, 1999; Lang, 2005; Minin et al., 2010*), the composite  
91 QRNN (CQRNN) (*Xu et al., 2017*), the expectile regression neural network (*Jiang et al., 2017*),  
92 and the generalized additive neural network (*Potts, 1999*). To the best of the author’s knowledge,  
93 the MCQRNN model is the first neural network-based implementation of quantile regression that  
94 guarantees non-crossing of regression quantiles.

95 The MCQRNN model is developed in Section 2, starting from the MMLP model, leading to  
96 the MQRNN model, and then finally to the full MCQRNN. Approaches to enforce monotonicity,  
97 positivity/non-negativity, and generalized additive model constraints, as well as to estimate un-  
98 certainty in the conditional  $\tau$ -quantile functions, are also provided. In Section 3, the MCQRNN  
99 model is compared via Monte Carlo simulation to standard MLP, QRNN, and CQRNN models  
100 using combinations of three functions and error distributions from *Xu et al. (2017)*. In Section 4,  
101 the MCQRNN model is applied to real-world climate data by estimating IDF curves at ungauged  
102 locations in Canada based on annual maximum rainfall series at neighbouring gauging stations.  
103 IDF curves, which are used in the design of civil infrastructure such as culverts, storm sewers,  
104 dams, and bridges, summarize the relationship between the intensity and occurrence frequency  
105 of extreme rainfall over averaging durations ranging from minutes to a day (*Canadian Standards*  
106 *Association, 2012*). The intensity of extreme rainfall, a non-negative quantity, should increase  
107 monotonically as the annual probability of occurrence decreases (e.g., from  $1 - \tau = 0.5$  to 0.01  
108 or, equivalently, a 2-yr to 100-yr return period) and as the storm duration decreases (e.g., from  
109 24-hr to 5-min). Monotonicity and positivity/non-negativity constraints are thus key features of  
110 an IDF curve. MCQRNN IDF curve estimates are compared with those obtained by fitting sepa-

111 rate QRNN models for each return period and duration, as done previously by *Ouali and Cannon*  
 112 (2017). Finally, Section 5 provides closing remarks and suggestions for future research.

## 113 2 Modelling framework

### 114 2.1 Monotone multi-layer perceptron (MMLP)

115 The monotone composite quantile regression neural network (MCQRNN) model starts with the  
 116 multi-layer perceptron (MLP) neural network with partial monotonicity constraints (*Zhang and*  
 117 *Zhang, 1999*) as its basis. For a data point with index  $t$ , the prediction  $\hat{y}(t)$  from a monotone  
 118 MLP (MMLP) is obtained as follows. First, the  $V$  covariates, each assumed to be standardized  
 119 to zero mean and unit standard deviation, are separated into two groups:  $x_{m \in M}(t)$  and  $x_{i \in I}(t)$  with  
 120 combined indices  $\{M \cup I \mid 1, \dots, V, V = (\#M + \#I)\}$ , where  $M$  is the set of indices for covariates with  
 121 a monotone increasing relationship with the prediction,  $I$  is the corresponding set of indices for  
 122 covariates without monotonicity constraints, and  $\#$  denotes the number of set elements. Covariates  
 123 are transformed into  $j = 1, \dots, J$  hidden layer outputs

$$h_j(t) = f \left( \sum_{m \in M} x_m(t) \exp(W_{mj}^{(h)}) + \sum_{i \in I} x_i(t) W_{ij}^{(h)} + b_j^{(h)} \right) \quad (1)$$

124 where  $\mathbf{W}^{(h)}$  is a  $V \times J$  parameter matrix,  $\mathbf{b}^{(h)}$  is a vector of  $J$  intercept parameters, and  $f$  is a smooth  
 125 non-decreasing function, usually taken to be the hyperbolic tangent function. Finally, the model  
 126 prediction is given as a weighted combination of the  $J$  hidden layer outputs

$$\hat{y}(t) = g \left( \sum_{j=1}^J h_j(t) \exp(w_j) + b \right) \quad (2)$$

127 where  $\mathbf{w}$  is a vector of  $J$  parameters,  $b$  is an intercept term, and  $g$  is a smooth non-decreasing  
 128 inverse-link function.

129 Because both  $f$  and  $g$  are non-decreasing, partial monotonicity constraints (i.e.,  $\frac{\partial \hat{y}}{\partial x_m} \geq 0$  every-  
 130 where) can be imposed by ensuring that all parameters leading from each monotone-constrained

131 covariate  $x_m$  are positive (Zhang and Zhang, 1999), in this case by applying the exponential func-  
 132 tion to the corresponding elements of  $\mathbf{W}^{(h)}$  and all elements of  $\mathbf{w}$ . Decreasing relationships can  
 133 be imposed by multiplying covariates by -1. Also, extra hidden layers of positive parameters can  
 134 be added to the model. As pointed out by Lang (2005) and Minin *et al.* (2010), an additional  
 135 hidden layer is required for the MMLP to maintain its universal function approximation capabili-  
 136 ties. While multiple hidden layers are included in the software implementation by Cannon (2017),  
 137 for sake of simplicity, this study only considers the single hidden layer architecture of Zhang and  
 138 Zhang (1999). In practice, simple functional relationships can still be represented by a single  
 139 hidden layer model.

140 If  $M$  is the empty set and the positivity constraint on the  $\mathbf{w}$  parameters is removed, this leads  
 141 to the standard MLP model. If  $f$  and  $g$  are the identity function, the MMLP reduces to a linear  
 142 model. If  $f$  is nonlinear, then the model can represent nonlinear relationships, including those  
 143 involving interactions between covariates; the number of hidden layer outputs  $J$  further controls  
 144 the potential complexity of the MLP mapping. All models in this study set  $f$  to be the hyperbolic  
 145 tangent function.

146 Adjustable parameters ( $\mathbf{W}^{(h)}$ ,  $\mathbf{b}^{(h)}$ ,  $\mathbf{w}$ ,  $b$ ) in the MMLP are set by minimizing the least squares  
 147 (LS) error function

$$E_{\text{LS}} = \frac{1}{N} \sum_{t=1}^N (y(t) - \hat{y}(t))^2 \quad (3)$$

148 over a training dataset with  $N$  data points  $\{(\mathbf{x}(t), y(t)) \mid t = 1, \dots, N\}$ , where  $y(t)$  is the target value  
 149 of the response variable. While LS regression is most common, different error functions are appro-  
 150 priate for different prediction tasks. Minimizing the LS error function is equivalent to maximum  
 151 likelihood estimation for the conditional mean assuming a Gaussian error distribution with con-  
 152 stant variance (i.e., a traditional regression task), while minimizing the least absolute error (LAE)  
 153 function

$$E_{\text{LAE}} = \frac{1}{N} \sum_{t=1}^N |y(t) - \hat{y}(t)| \quad (4)$$

154 leads to a regression estimate for the conditional median (i.e., the  $\tau = 0.5$ -quantile) (*Koenker and*  
 155 *Bassett Jr., 1978*).

## 156 **2.2 Monotone quantile regression neural network (MQRNN)**

157 The fundamental quantity of interest here is not just the median, but rather predictions  $\hat{y}_\tau(t)$  of  
 158 the conditional quantile associated with the quantile probability  $\tau$  ( $0 < \tau < 1$ ). In this context,  
 159 combining the MMLP architecture from Section 2.1, as given by equations 1 and 2,

$$\hat{y}_\tau(t) = g \left[ \sum_{j=1}^J f \left( \sum_{m \in M} x_m(t) \exp(W_{mj}^{(h)}) + \sum_{i \in I} x_i(t) W_{ij}^{(h)} + b_j^{(h)} \right) \exp(w_j) + b \right], \quad (5)$$

160 with the quantile regression error function

$$E_\tau = \frac{1}{N} \sum_{t=1}^N \rho_\tau(y(t) - \hat{y}_\tau(t)) \quad (6)$$

161 where

$$\rho_\tau(\varepsilon) = \begin{cases} \tau \varepsilon & \varepsilon \geq 0 \\ (\tau - 1) \varepsilon & \varepsilon < 0 \end{cases} \quad (7)$$

162 leads to estimates  $\hat{y}_\tau$  of the conditional  $\tau$ -quantile function (*Koenker and Bassett Jr., 1978*). The  
 163 resulting model is referred to as the MQRNN. When  $\tau = 0.5$ , equation 6 is, up to a constant scaling  
 164 factor, the same as the LAE function (equation 4) that yields the conditional median; for  $\tau \neq 0.5$ ,  
 165 the asymmetric absolute value function gives different weight to positive/negative deviations. For  
 166 example, fitting a model with  $\tau = 0.95$  provides an estimate for the conditional 95<sup>th</sup>-percentile,  
 167 i.e., a covariate-dependent probability of exceedance of 5%. Relaxing the monotonicity constraints  
 168 gives the standard QRNN model as presented by *Cannon (2011)*.



169 Parameters can be estimated by a gradient-based nonlinear optimization algorithm, with cal-  
170 culation of the gradient using backpropagation; given the simple relationship between equations 4  
171 and 6, the analytical expression for the gradient of the quantile regression error function follows  
172 from that of the LAE function (*Hanson and Burr, 1988*). In this case, the derivative is undefined at  
173 the origin, which means that a smooth approximation is instead substituted for the exact quantile  
174 regression error function. Following *Chen (2007)* and *Cannon (2011)*, a Huber-norm version of  
175 equation 7 replaces  $\rho_\tau(\varepsilon)$  in the quantile regression error function. This approximation, denoted  
176 by (A), is given by

$$\rho_\tau^{(A)}(\varepsilon) = \begin{cases} \tau \varphi(\varepsilon) & \varepsilon \geq 0 \\ (\tau - 1) \varphi(\varepsilon) & \varepsilon < 0 \end{cases} \quad (8)$$

177 where the Huber function

$$\varphi(\varepsilon) = \begin{cases} \frac{\varepsilon^2}{2\alpha} & 0 \leq |\varepsilon| \leq \alpha \\ |\varepsilon| - \frac{\alpha}{2} & |\varepsilon| > \alpha \end{cases} \quad (9)$$

178 is a hybrid of the absolute value and squared error functions (*Huber, 1964*).

179 The Huber function transitions smoothly from the squared error, which is applied around the  
180 origin ( $\pm\alpha$ ) to ensure differentiability, and the absolute error. As  $\alpha \rightarrow 0$ , the approximate er-  
181 ror function converges to the exact quantile regression error function. It should be noted that a  
182 slightly different approximation is used by *Muggeo et al. (2012)*. Based on experimental results  
183 (not shown), both approximations ultimately provide models that are indistinguishable. However,  
184 the Huber function approximation is used here for its added ability to emulate the LS cost func-  
185 tion. For sufficiently large  $\alpha$ , all model deviations are squared and the approximate error function  
186 instead becomes an asymmetric version of the LS error function (equation 3). For  $\tau = 0.5$  and  
187 large  $\alpha$ , the error function is symmetric and is, up to a constant scaling factor, equal to the LS error  
188 function. For  $\tau \neq 0.5$ , the asymmetric LS error function results in an estimate of the conditional  
189 expectile function (*Newey and Powell, 1987; Yao and Tong, 1996; Waltrup et al., 2015*). Hence,

190 depending on values of  $\alpha$  and  $\tau$ , minimizing the approximate quantile regression error function can  
 191 provide regression estimates for the conditional mean ( $\alpha \gg 0$ ,  $\tau = 0.5$ ), median ( $\alpha \rightarrow 0$ ,  $\tau = 0.5$ ),  
 192 quantiles ( $\alpha \rightarrow 0$ ,  $0 < \tau < 1$ ), and expectiles ( $\alpha \gg 0$ ,  $0 < \tau < 1$ ) (Jiang *et al.*, 2017). Unless noted  
 193 otherwise, all subsequent references to  $\rho_\tau^{(A)}$  and  $E_\tau^{(A)}$  will refer to the conditional quantile form of  
 194 the Huber function approximation.

195 Unlike linear regression, where the total number of model parameters is limited by the number  
 196 of covariates  $V$ , the complexity of the MQRNN model also depends on the number of hidden layer  
 197 outputs  $J$ . Model complexity, and hence  $J$ , should be set such that the model can generalize to  
 198 new data, which, in practice, usually means avoiding overfitting to noise in the training dataset.  
 199 Additionally, regularization terms that penalize the magnitude of the parameters, hence limiting  
 200 the nonlinear modelling capability of the model, can be added to the error function

$$\tilde{E}_\tau^{(A)} = E_\tau^{(A)} + \lambda^{(h)} \frac{1}{VJ} \sum_{i=1}^V \sum_{j=1}^J \left( W_{ij}^{(h)} \right)^2 + \lambda \frac{1}{J} \sum_{j=1}^J (w_j)^2 \quad (10)$$

201 where  $\lambda^{(h)} \geq 0$  and  $\lambda \geq 0$  are hyperparameters that control the size of the penalty applied to the  
 202 elements of  $\mathbf{W}^{(h)}$  and  $\mathbf{w}$  respectively. Values of  $J$  and, optionally, the  $\lambda^{(h)}$  and  $\lambda$  hyperparame-  
 203 ters are typically set by minimizing out-of-sample generalization error, for example as estimated  
 204 via cross-validation or modified versions of an information criterion like the Akaike information  
 205 criterion (QAIC) (Koenker and Schorfheide, 1994; Doksum and Koo, 2000)

$$\text{QAIC} = -2 \log(E_\tau) + 2p \quad (11)$$

207 where  $p$  is an estimate of the effective number of model parameters.

### 208 **2.3 Monotone composite quantile regression neural network (MCQRNN)**

209 The MQRNN model in Section 2.2 is specified for a single  $\tau$ -quantile; no efforts are made to  
 210 avoid quantile crossing for multiple estimates. To date, the simultaneous estimation of multiple  
 211  $\tau$ -quantiles with guaranteed non-crossing has not been possible for QRNN models. However, si-  
 212 multaneous estimates for multiple values of  $\tau$  are used in the composite QRNN (CQRNN) model

213 proposed by *Xu et al. (2017)*. CQRNN shares the same goal as the linear composite quantile re-  
 214 gression (CQR) model (*Zou and Yuan, 2008*), namely to borrow strength across multiple regression  
 215 quantiles to improve the estimate of the true, unknown relationship between the covariates and the  
 216 response. This is especially valuable in situations where the error follows a heavy-tailed distribu-  
 217 tion. In CQR, the regression coefficients are shared across the different quantile regression mod-  
 218 els. Similarly, in CQRNN, the  $\mathbf{W}^{(h)}$ ,  $\mathbf{b}^{(h)}$ ,  $\mathbf{w}$ ,  $b$  parameters are shared across the different QRNN  
 219 models. Hence, the models are not explicitly trying to describe the full conditional response dis-  
 220 tribution, but rather a single  $\tau$ -independent function that best describes the true covariate-response  
 221 relationship. Structurally, the CQRNN model is the same as the QRNN model. The only difference  
 222 is the quantile regression error function, which is now summed over  $K$  (usually equally spaced)  
 223 values of  $\tau$

$$E_{C\tau}^{(A)} = \frac{1}{KN} \sum_{k=1}^K \sum_{t=1}^N \rho_{\tau_k}^{(A)} (y(t) - \hat{y}_{\tau_k}(t)) \quad (12)$$

224 where, for example,  $\tau_k = \frac{k}{K+1}$  for  $k = 1, 2, \dots, K$ . Penalty terms can be added as in equation 10.

225 The MCQRNN model combines the MQRNN model architecture given by equation 5 with the  
 226 composite quantile regression error function (equation 12) to simultaneously estimate non-crossing  
 227 regression quantiles. To show how this is achieved, consider an  $N \times \#I$  matrix of covariates  $\mathbf{X}$ , a  
 228 corresponding response vector  $\mathbf{y}$  of length  $N$ , and the goal of estimating non-crossing quantile  
 229 functions for  $\tau_1 < \tau_2 < \dots < \tau_K$ . First, create a new  $\#M = 1$  monotone covariate vector  $\mathbf{x}_m^{(S)}$  of  
 230 length  $S = KN$ , where  $(S)$  denotes stacked data, by repeating each of the  $K$  specified  $\tau$  values  $N$   
 231 times and stacking. Next, stack  $K$  copies of  $\mathbf{X}$  and concatenate with  $\mathbf{x}_m^{(S)}$  to form a stacked covariate  
 232 matrix  $\mathbf{X}^{(S)}$  of dimension  $S \times (1 + \#I)$ . Finally stack  $K$  copies of  $\mathbf{y}$  to form  $\mathbf{y}^{(S)}$ . Taken together,  
 233 this gives the stacked dataset

$$\mathbf{X}^{(S)} = \begin{bmatrix} \tau_1 & x_1(1) & \cdots & x_{\#I}(1) \\ \vdots & \vdots & \ddots & \vdots \\ \tau_1 & x_1(N) & \cdots & x_{\#I}(N) \\ \tau_2 & x_1(1) & \cdots & x_{\#I}(1) \\ \vdots & \vdots & \ddots & \vdots \\ \tau_2 & x_1(N) & \cdots & x_{\#I}(N) \\ \vdots & \vdots & \vdots & \vdots \\ \tau_K & x_1(1) & \cdots & x_{\#I}(1) \\ \vdots & \vdots & \ddots & \vdots \\ \tau_K & x_1(N) & \cdots & x_{\#I}(N) \end{bmatrix}, \mathbf{y}^{(S)} = \begin{bmatrix} y(1) \\ \vdots \\ y(N) \\ y(1) \\ \vdots \\ y(N) \\ \vdots \\ y(1) \\ \vdots \\ y(N) \end{bmatrix} \quad (13)$$

234 which is used to fit the MQRNN model. By treating the  $\tau$  values as a monotone covariate, pre-  
 235 dictions  $\hat{y}_\tau^{(S)}$  from equation 5 for fixed values of the non-monotone covariates are guaranteed to  
 236 increase with  $\tau$ . Non-crossing is imposed by construction. Defining  $\tau(s) = x_1^{(S)}(s)$ , the composite  
 237 quantile regression error function for the stacked data can be written as

$$E_{C\tau}^{(A,S)} = \sum_{s=1}^S \omega_{\tau(s)} \rho_{\tau(s)}^{(A)} \left( y^{(S)}(s) - \hat{y}_{\tau(s)}^{(S)}(s) \right) \quad (14)$$

238 where  $\omega_{\tau(s)}$  are weights that can be used to allow regression quantiles for each  $\tau_k$  to contribute  
 239 different amounts to the total error (*Jiang et al., 2012; Sun et al., 2013*); constant weights  $\omega_{\tau(s)} =$   
 240  $1/S$  lead to the standard composite quantile regression error function. Minimization of equation  
 241 14 results in the fitted MCQRNN model. (Note: non-crossing expectile regression models can  
 242 be obtained by adjusting  $\alpha \gg 0$  in  $\rho_\tau^{(A)}$ .) Following model estimation, conditional  $\tau$ -quantile  
 243 functions can be predicted for any value of  $\tau_1 \leq \tau \leq \tau_K$  by entering the desired value of  $\tau$  into the  
 244 monotone covariate.

245 To illustrate, Figure 1 shows results from a MCQRNN model ( $J = 4$ ,  $\lambda^{(h)} = 0.00001$ ,  $\lambda = 0$ ,  
 246  $K = 9$ ,  $\tau = 0.1, 0.2, \dots, 0.9$ ) fit to 500 samples of synthetic data for the two functions from *Bondell*  
 247 *et al. (2010)*

$$y_1 = 0.5 + 2x + \sin(2\pi x - 0.5) + \varepsilon \quad (15)$$

248 and

$$y_2 = 3x + [0.5 + 2x + \sin(2\pi x - 0.5)] \varepsilon \quad (16)$$

249 where  $x$  is drawn from the standard uniform distribution  $x \sim U(0, 1)$  and  $\varepsilon$  from the standard  
 250 normal distribution  $\varepsilon \sim N(0, 1)$ . All  $\tau$  are weighted equally in equation 14 (i.e., values of  $\omega_{\tau(s)}$   
 251 are constant). Results are compared with those from separate QRNN models ( $J = 4$  and  $\lambda^{(h)} =$   
 252  $0.00001$ ) for each  $\tau$ -quantile. Quantile curves cross for QRNN, especially at the boundaries of  
 253 the training data, whereas the MCQRNN model is able to simultaneously estimate multiple non-  
 254 crossing quantile functions that correspond more closely to the true conditional quantile functions.  
 255 While quantile crossing in QRNN models can be minimized by selecting and applying a suitable  
 256 weight penalty (*Cannon, 2011*), non-crossing cannot be guaranteed, whereas MCQRNN models  
 257 impose this constraint by construction.

258

[Figure 1 about here.]

## 259 **2.4 Additional constraints and uncertainty estimates**

260 As mentioned above, constraints in addition to non-crossing of quantile functions may be useful  
 261 for some MCQRNN modelling tasks. Partial monotonicity constraints for specified covariates can  
 262 be imposed as described in Section 2.1; positivity or non-negativity constraints can be added by  
 263 setting  $g$  in equation 2 to the exponential or smooth ramp function (*Cannon, 2011*), respectively;  
 264 and covariate interactions can be restricted by the approach described in Appendix 1.

265 A form of the parametric bootstrap can be used to estimate uncertainty in the conditional  $\tau$ -  
 266 quantile functions. While the MCQRNN model is explicitly optimized for  $K$  specified values  
 267 of  $\tau$ , the use of the quantile probability as a monotone covariate means that conditional  $\tau$ -quantile  
 268 functions can be interpolated for any value of  $\tau_1 \leq \tau \leq \tau_K$ . Proper distribution, probability density,

269 and quantile functions can then be constructed by assuming a parametric form for the tails of the  
 270 distribution (*Quiñonero Candela et al., 2006; Cannon, 2011*). The parametric bootstrap proceeds  
 271 by drawing random samples from the resulting conditional distribution, refitting the MCQRNN  
 272 model, making estimates of the conditional  $\tau$ -quantiles, and repeating many times. Confidence  
 273 intervals are estimated from the bootstrapped conditional  $\tau$ -quantiles.

274 For illustration, examples of MCQRNN model outputs with positivity and monotonicity con-  
 275 straints, as well as confidence intervals obtained by the parametric bootstrap, are shown in Figure  
 276 2 for the two *Bondell et al. (2010)* functions.

277 [Figure 2 about here.]

### 278 3 Monte Carlo simulation

279 Given the close relationship between the MCQRNN and CQRNN models, performance is first  
 280 assessed via Monte Carlo simulation using the experimental setup adopted by *Xu et al. (2017)* for  
 281 CQRNN. The MCQRNN model is compared with standard MLP, QRNN, and CQRNN models on  
 282 datasets generated for three example functions:

$$(example 1) \quad y = \sin(2x_1) + 2 \exp(-16x_2^2) + 0.5\epsilon \quad (17)$$

283 where  $x_1 \sim N(0, 1)$  and  $x_2 \sim N(0, 1)$ ;

$$(example 2) \quad y = (1 - x + 2x^2) \exp(-0.5x^2) + \frac{(1 + 0.2x)}{5} \epsilon \quad (18)$$

284 where  $x \sim U(-4, 4)$ ; and

$$(example 3) \quad y = \frac{40 \exp\{8[(x_1 - 0.5)^2 + (x_2 - 0.5)^2]\}}{\exp\{8[(x_1 - 0.2)^2 + (x_2 - 0.7)^2]\} + \exp\{8[(x_1 - 0.7)^2 + (x_2 - 0.7)^2]\}} + \epsilon \quad (19)$$

285 where  $x_1 \sim U(0, 1)$  and  $x_2 \sim U(0, 1)$ . For each of the three functions, random errors are generated  
286 from three different distributions: the normal distribution  $\varepsilon \sim N(0, 0.25)$ , Student’s t distribution  
287 with three degrees of freedom  $\varepsilon \sim t(3)$ , and the chi-squared distribution with three degrees of  
288 freedom  $\varepsilon \sim \chi^2(3)$ . Monte Carlo simulations are performed for the nine resulting datasets.

289 To evaluate the benefit of adding MCQRNN’s non-crossing constraint to the simultaneous es-  
290 timation of multiple regression quantiles, a second variant of CQRNN, referred to as CQRNN\*,  
291 is included in the comparison. The CQRNN\* model takes the same structure as MCQRNN, i.e.,  
292 with  $\tau$  values included as an extra input variable (equation 13). However, partial monotonicity  
293 constraints are removed from the  $\tau$ -covariate; the exponential function is no longer applied to the  
294 relevant elements in  $\mathbf{W}^{(h)}$  and all elements of  $\mathbf{w}$ . The resulting model provides estimates of multi-  
295 ple regression quantiles, but crossing can now occur. This differs from the CQRNN model of *Xu*  
296 *et al.* (2017), which estimates a single regression equation using the composite QR cost function,  
297 and MCQRNN, which additionally guarantees non-crossing of the multiple regression quantiles.  
298 Differences between the three models are illustrated in Figure 3 on the example 2 dataset with  
299  $\varepsilon \sim \chi^2(3)$  distributed noise.

300 [Figure 3 about here.]

301 For each example and error distribution in the Monte Carlo simulations, 400 samples are gen-  
302 erated and split randomly into 200 training and 200 testing samples. Results for QRNN, MLP,  
303 CQRNN, CQRNN\*, and MCQRNN models are compared by fitting to the training samples and  
304 evaluating on the testing samples. Simulations are repeated 1000 times. Following *Xu et al.* (2017),  
305 the number of hidden layer outputs in all models is set to  $J = 4$  for example 1 and  $J = 5$  for ex-  
306 amples 2 and 3; for sake of simplicity, no weight penalty terms are added when fitting any of the  
307 models. (When comparing results with those reported by *Xu et al.*, 2017, note that omitting weight  
308 penalty regularization here leads to smaller inter-model differences in performance within both the  
309 training and testing samples, which suggests potential instability in hyperparameter selection in the  
310 previous study.) The goal is to estimate the true functional relationship specified by equations 17 to  
311 19. The QRNN model is fit for  $\tau = 0.5$ , whereas CQRNN, CQRNN\*, and MCQRNN models use

312  $K = 19$  equally spaced values of  $\tau$ . In the case of CQRNN\* and MCQRNN, evaluations are based  
313 on an estimate of the conditional mean function obtained by taking the mean over predictions for  
314 the  $K = 19$   $\tau$ -quantiles. Performance is measured by the root mean squared error (RMSE) between  
315 model predictions for the test samples and the actual values of  $y$ . For reference, training RMSE is  
316 also reported. Results are shown in Figure 4.

317 [Figure 4 about here.]

318 As expected, the MLP model, which is fit using the LS error function and hence is optimal  
319 for normally distributed errors with constant variance, tends to perform best for the three exam-  
320 ples when  $\varepsilon \sim N(0, 0.25)$ . Differences are, however, small for both training and testing datasets.  
321 Median RMSE values for each of the models fall within 10% of MLP in all cases and the 90% inter-  
322 percentile ranges are typically comparable. For the two non-normal error distributions,  $\varepsilon \sim t(3)$   
323 and  $\varepsilon \sim \chi^2(3)$ , CQRNN\* and MCQRNN models tend to outperform the other models on the test-  
324 ing datasets. Again, differences in median testing RMSE are small, especially among the QRNN-  
325 based models. In general, however, MLP performs worst, followed by QRNN and CQRNN, with  
326 CQRNN\* and MCQRNN offering slight improvements. In terms of robustness, as measured by  
327 the 5th and 95th percentiles of testing RMSE, MLP is clearly least robust, while MCQRNN tends  
328 to perform best, especially for example 3. For this example and the two non-normal error distri-  
329 butions, MCQRNN also outperforms CQRNN\*, which points to added value of the non-crossing  
330 constraint. Overall, the MCQRNN model performs well on the synthetic data from *Xu et al. (2017)*.  
331 In the next section, the modelling framework is applied to real-world climate data. As a proof of  
332 concept, rainfall IDF curves are estimated by MCQRNN at ungauged locations in Canada and,  
333 following *Ouali and Cannon (2017)*, results are compared against those obtained from QRNN  
334 models.



## 4 Rainfall IDF curves

### 4.1 Data

The design of some civil infrastructure – hydraulic, hydrological, and water resource structures – is based on the design flood, which is the flood hydrograph associated with a specified frequency of occurrence or return period. In the absence of gauged discharge data, rainfall data are instead used to generate a design storm, which can then be transformed into synthetic peak streamflows for the return period of interest. The design storm provides the temporal distribution of rainfall intensities associated with a specified return period and duration. The necessary information on the frequency of occurrence, duration, and intensity of rainstorms is compactly summarized in an IDF curve, and hence IDF curves are key sources of information for engineering design applications. IDF curves provided by Environment and Climate Change Canada (ECCC) summarize the relationship between annual maximum rainfall intensity for specified frequencies of occurrence (2-, 5-, 10-, 25-, 50-, and 100-yr return periods, i.e.,  $\tau = 0.5, 0.8, 0.9, 0.96, 0.98, 0.99$ -quantiles) and durations ( $D = 5\text{-}, 10\text{-}, 15\text{-}, 30\text{-}, 60\text{-min}, 2\text{-}, 6\text{-}, 12\text{-}, \text{ and } 24\text{-hr}$ ) at locations in Canada with long records of short-duration rainfall rate observations. Annual maximum rainfall rate data for durations from 5-min to 24-hr are archived by ECCC as part of the Engineering Climate Datasets (*Environment and Climate Change Canada, 2014*). The rainfall rate dataset is based on tipping bucket rain gauge observations at 565 stations across Canada (Figure 5). Record lengths range from 10-yr to 81-yr, with a median length of 25-yr. Information on the observing program, quality control, and quality assurance methods is provided in detail by *Shephard et al. (2014)*.

[Figure 5 about here.]

Official ECCC IDF curves are constructed by first fitting the parametric Gumbel distribution to annual maximum rainfall rate series at each site for each duration. At the majority of stations, the actual curves are then based on best fit linear interpolation equations between log-transformed duration and log-transformed Gumbel quantiles for each of the specified return periods. For reference, IDF curves for Victoria Intl A, a station on the southwest coast of British Columbia, Canada,

361 are shown in Figure 6. Points indicate return values of rainfall intensity obtained from the fitted  
362 Gumbel distribution for each combination of return period and duration; the IDF curves for each  
363 return period are based on log-log interpolating equations through these points, and hence plot as  
364 straight lines.

365 [Figure 6 about here.]

366 Naturally, the ECCC approach cannot provide quantile estimates for locations where short-  
367 duration rainfall observations are not recorded or available. Parametric extreme value distributions,  
368 fit in conjunction with regionalization or regional regression models, have been used to estimate  
369 IDF curves at ungauged locations in Canada by *Alila (1999, 2000)*, *Kuo et al. (2012)*, and *Mail-*  
370 *hot et al. (2013)*. As a non-parametric alternative to standard parametric approaches, *Ouali and*  
371 *Cannon (2017)* recently evaluated regional QRNN models for IDF curves at ungauged locations.  
372 While results suggest that the QRNN model can outperform standard parametric methods, further  
373 improvements are still possible. In particular, *Ouali and Cannon (2017)* fit separate QRNN models  
374 for each  $\tau$ -quantile and duration, which means that quantile crossing is possible; further, rainfall  
375 intensities may not increase as storm duration decreases. Instead, use of the MCQRNN is proposed  
376 to ensure non-crossing quantiles and a monotone decreasing relationship with increasing storm du-  
377 ration. Estimation at ungauged sites typically relies on pooling gauged data from a homogeneous  
378 region around the site of interest, whether in geographic space or some derived hydroclimatologi-  
379 cal space (*Ouarda et al., 2001*), and then fitting a regression model linking spatial covariates with  
380 the short-duration rainfall rate response. As the focus of this study is on methods for conditional  
381 quantile estimation, and not the delineation of homogeneous regions, regionalizations here are  
382 based on a simple geographic region-of-influence (*Burn, 1990*) in which data from the 80 nearest  
383 gauged sites are pooled together to form the training dataset for the site of interest. Following  
384 *Aziz et al. (2014)*, this emphasizes the use of data from a large number of sites rather than the  
385 most homogeneous sites; it is then up to the regression model to infer relevant covariate-response  
386 relationships from within this larger pool of data. In areas with low station density, however, it is  
387 questionable whether any statistical regional frequency analysis technique can be used to reliably

388 estimate rainfall extremes. Performance in sparsely monitored regions will be explored as part of  
 389 the subsequent model evaluation.

390 Based on this experimental design, observed short-duration rainfall rate data  $i_D$  for multiple  
 391 durations  $D$  are used as the response variable in the MCQRNN model and spatial variables avail-  
 392 able over the domain – including at the ungauged location – are used as covariates in the regression  
 393 equations. In this study, five covariates ( $\#I = 5$ ), including latitude (lat), longitude (lon), elevation  
 394 (elev), and climatological total winter (DJF) and summer precipitation (JJA) (Figure 5) (*McKenney*  
 395 *et al.*, 2011), are used alongside the two ( $\#M = 2$ ) monotone covariates [ $\tau$  and  $-\log(D)$ ]. As an  
 396 abbreviated example, stacked data matrices for a single site ( $s_1$ ), two quantiles ( $\tau_1$  and  $\tau_2$ ), and two  
 397 durations ( $D_1$  and  $D_2$ ), for  $N$  years of short-duration rainfall observations would take the form:

$$\mathbf{y}_{s_1}^{(S)} = \begin{bmatrix} i_{D_1}(1) \\ \vdots \\ i_{D_1}(N) \\ i_{D_2}(1) \\ \vdots \\ i_{D_2}(N) \\ i_{D_1}(1) \\ \vdots \\ i_{D_1}(N) \\ i_{D_2}(1) \\ \vdots \\ i_{D_2}(N) \end{bmatrix}, \mathbf{X}_{s_1}^{(S)} = \begin{bmatrix} \tau_1 & -\log(D_1) & \text{lat}(s_1) & \text{lon}(s_1) & \text{elev}(s_1) & \text{DJF}(s_1) & \text{JJA}(s_1) \\ \vdots & \vdots & \vdots & \vdots & \vdots & \vdots & \vdots \\ \vdots & -\log(D_1) & \vdots & \vdots & \vdots & \vdots & \vdots \\ \vdots & -\log(D_2) & \vdots & \vdots & \vdots & \vdots & \vdots \\ \vdots & \vdots & \vdots & \vdots & \vdots & \vdots & \vdots \\ \tau_1 & -\log(D_2) & \vdots & \vdots & \vdots & \vdots & \vdots \\ \tau_2 & -\log(D_1) & \vdots & \vdots & \vdots & \vdots & \vdots \\ \vdots & \vdots & \vdots & \vdots & \vdots & \vdots & \vdots \\ \vdots & -\log(D_1) & \vdots & \vdots & \vdots & \vdots & \vdots \\ \vdots & -\log(D_2) & \vdots & \vdots & \vdots & \vdots & \vdots \\ \vdots & \vdots & \vdots & \vdots & \vdots & \vdots & \vdots \\ \tau_2 & -\log(D_2) & \text{lat}(s_1) & \text{lon}(s_1) & \text{elev}(s_1) & \text{DJF}(s_1) & \text{JJA}(s_1) \end{bmatrix}. \tag{20}$$

398 For a given site of interest, the full stacked training dataset is expanded to include data from the  
399 80 nearest gauged sites, 6 values of  $\tau$ (0.5, 0.8, 0.9, 0.96, 0.98, 0.99), and 9 durations (5-, 10-, 15-,  
400 30-, 60-min, 2-, 6-, 12-, and 24-hr).

## 401 **4.2 Cross-validation results**

402 Regional MCQRNN and QRNN models for IDF curves are evaluated via leave-one-out cross-  
403 validation. Each of the 565 observing sites is treated, in turn, as being “ungauged”, i.e., data from  
404 nearest 80 sites to each left-out site are used to fit the models, model predictions are made at the  
405 left-out site, and model performance statistics are calculated based on the left-out data. Following  
406 *Ouali and Cannon (2017)*, 54 separate QRNN models are fit for each site, one for each combination  
407 of the 9 durations ( $D = 5\text{-min to } 24\text{-hr}$ ) and 6  $\tau$ -quantiles ( $\tau = 0.5$  to  $0.99$ ) reported in ECCC IDF  
408 curves. Each MCQRNN model combines data for all 9 values of  $D$  and fits non-crossing quantile  
409 curves for the 6  $\tau$ -quantiles simultaneously.

410 Non-negativity constraints are imposed in both QRNN and MCQRNN models by setting  $g$   
411 to the smooth ramp function (*Cannon, 2011*). Monotonicity constraints – increasing with  $\tau$  and  
412 decreasing with  $D$  – are imposed in the MCQRNN model by adopting the MMLP architecture  
413 with additional monotone covariates [ $\tau$  and  $-\log(D)$ ]. The optimum level of complexity for each  
414 kind of model is selected based on values of QAIC, here based on the composite QR error function  
415 (e.g., *Xu et al., 2017*), averaged over all sites, from candidates with  $J = 1, 2, \dots, 5$  (*Koenker and*  
416 *Schorfheide, 1994; Doksum and Koo, 2000; Xu et al., 2017*). The number of hidden nodes  $J$  is  
417 fixed to the same value for all sites in the study domain. QAIC is minimized for QRNN models  
418 with  $J = 1$  and MCQRNN models with  $J = 3$ .

419 [Table 1 about here.]

420 Cross-validation results comparing the MCQRNN ( $J = 3$ ) and QRNN ( $J = 1$ ) models are  
421 reported in terms of relative differences in leave-one-out estimates of the quantile regression error  
422 function

$$RD_{\tau} = 100 \left( \frac{E_{\tau}^{(\text{MCQRNN})} - E_{\tau}^{(\text{QRNN})}}{E_{\tau}^{(\text{QRNN})}} \right) \quad (21)$$

423 summed over all stations for each return period and duration. Values are shown in Table 1a.  
 424 Because the underlying model architecture is, aside from different values of  $J$  and inclusion of  
 425 monotonicity constraints, fundamentally the same for the QRNN and MCQRNN models, it is  
 426 not surprising that the two perform similarly well. MCQRNN and QRNN errors fall within 5%  
 427 of one another for nearly all combinations of return period and duration, although MCQRNN  
 428 tends to perform slightly better for short durations ( $D = 5\text{-min to 2-hr}$ ) and QRNN for longer  
 429 durations ( $D = 6\text{-hr to 24-hr}$ ). Poorer performance of the MCQRNN model in these cases is partly  
 430 attributable to the smaller rainfall intensities that are associated with long duration storms being  
 431 weighted less in the CQR cost function (equation 14) than the larger intensities that accompany  
 432 short duration storms. This can be remedied by setting  $\omega_{\tau(s)} \propto \log(D)$  in equation 14. Results  
 433 for the MCQRNN model with weighting are shown in Table 1b. Weighting improves performance  
 434 for longer durations, while having minimal impact on shorter durations. Further results will be  
 435 reported for the weighted MCQRNN model.

436 Despite the similar levels of quantile error, the additional MCQRNN monotonicity constraints  
 437 on  $\tau$  and  $D$  leads to IDF curves that are guaranteed to increase as occurrence frequency and storm  
 438 duration decrease, properties that need not be present for QRNN predictions. This is evident for  
 439 Victoria Intl A (Figure 7), where quantile crossing and non-monotone increasing behaviour with  
 440 decreasing storm duration is noted for the 100-yr QRNN model predictions (cf. Figure 6).

441 [Figure 7 about here.]

442 Each of the QRNN ( $J = 1$ ) models for the 54 combinations of  $\tau$  and  $D$  contain  $J(\#I + 1) + J +$   
 443  $1 = 1(5 + 1) + 1 + 1 = 8$  parameters or 432 parameters in total. Because it borrows strength over  
 444  $\tau$  and  $D$  ( $\#M = 2$ ), the MCQRNN ( $J = 3$ ) model requires just  $J(\#I + \#M + 1) + J + 1 = 3(5 + 2 +$   
 445  $1) + 3 + 1 = 28$  shared parameters for the same task. Given that the two models show similar levels  
 446 of performance, parameters in the separate QRNN equations must be largely redundant. If model

447 complexity is increased, for example to  $J = 5$ , the total number of estimated parameters is 1,944 for  
 448 QRNN (36 for each combination of  $\tau$  and  $D$ ) versus 46 for MCQRNN. By way of comparison, the  
 449 at-site (rather than ungauged) ECCC IDF curves require estimation of 30 parameters (18 Gumbel  
 450 distribution and 12 interpolation equation parameters).

451 [Figure 8 about here.]

452 Do the non-crossing/monotonicity constraints and ability to borrow strength provide a guard  
 453 against overfitting if MCQRNN model complexity is misspecified? Figure 8 shows relative dif-  
 454 ferences  $RD_\tau$  in cross-validated quantile regression error for MCQRNN and QRNN models with  
 455  $J = 1, 2, \dots, 5$ ; in both cases, the optimal QRNN ( $J = 1$ ) model serves as the reference. Consis-  
 456 tent with results from QAIC model selection, cross-validated QRNN errors increase when  $J > 1$ .  
 457 When using more than the recommended number of hidden nodes, the QRNN performs poorly,  
 458 especially for long return period estimates. However, for MCQRNN, in the absence of underfitting  
 459 (i.e.,  $J = 1$ ), there is little penalty for specifying an overly complex model. Performance of the  
 460 optimal MCQRNN ( $J = 3$ ) model recommended by QAIC model selection is nearly identical to  
 461 that of the misspecified  $J = 5$  model. The non-crossing constraint provides strong regularization  
 462 and resistance to overfitting.

463 [Table 2 about here.]

464 Results reported so far have compared leave-one-out cross-validation performance of the MC-  
 465 QRNN and QRNN models. This does not provide any indication of how well the ungauged pre-  
 466 dictions compare with those estimated by the at-site ECCC IDF curve procedure, i.e., by fitting  
 467 the Gumbel distribution and log linear interpolating equations to observed annual maxima at each  
 468 station. Following *Ouali and Cannon (2017)*, the ability of the MCQRNN to replicate the at-site  
 469 ECCC IDF curves is measured by the quantile regression error ratio

$$R_\tau = \frac{E_\tau^{(ECCC)}}{E_\tau^{(MCQRNN)}} \quad (22)$$

470 where  $E_{\tau}^{(ECCC)}$  is the in-sample, at-site quantile regression error of the ECCC IDF curve interpo-  
471 lating equations. A value of 1 means that ungauged MCQRNN predictions reach the same level  
472 of error as the at-site ECCC IDF curves. Note: even though the ECCC IDF curves are calculated  
473 from observations at each station, it is possible for  $R_{\tau}$  to exceed 1 as the annual maximum rainfall  
474 data may deviate from the assumed Gumbel distribution and log linear form of the interpolating  
475 equations. Results are summarized in Table 2. Values of  $R_{\tau}$  greater than 0.9 – based on the 10%  
476 relative error threshold recommended by *Mishra et al.* (2012) for acceptable model simulations  
477 of urban rainfall extremes – are found for 41 of the 54 combinations of  $D$  and  $\tau$ , including all  
478 return periods from 2-yr to 10-yr. More broadly, values exceed 0.7 for all combinations of  $D$  and  
479  $\tau$ .

480 [Figure 9 about here.]

481 As shown in Figure 5, stations are not evenly distributed across Canada; northern latitudes,  
482 in particular, are very sparsely gauged. Does MCQRNN performance depend on station density?  
483 Values of  $R_{\tau}$ , stratified by the median distance of each ungauged station to its 80 neighbours, are  
484 shown in Figure 9. As expected, errors are nearly equivalent ( $R_{\tau} > 0.975$ ) to the at-site estimates  
485 in areas of high station density (median distances  $< 100$ -km). Modest performance declines are  
486 noted ( $R_{\tau} > 0.875$ ) with increasing median distance up to 500-km, beyond which performance  
487 degrades more substantially, especially for the longest return periods ( $R_{\tau=0.99} < 0.8$ ). The viability  
488 of ungauged estimation should be evaluated carefully in areas of low station density.

## 489 5 Conclusion

490 This study introduces a novel form of quantile regression that can be used to simultaneously es-  
491 timate multiple non-crossing, nonlinear quantile regression functions. MCQRNN is the first neu-  
492 ral network-based quantile regression model that guarantees non-crossing of regression quantiles.  
493 The model architecture, which is based on the standard MLP neural network, also allows optional  
494 monotonicity, positivity/non-negativity, and generalized additive model constraints to be imposed

495 in a straightforward manner. As an extension, a simple way to control the strength of non-additive  
496 relationships is also provided. The Huber function approximation to the QR error function means  
497 that standard least-squares regression and non-crossing expectile regression functions can be esti-  
498 mated using the same model architecture.

499 Given its close relationship to composite QR models, MCQRNN is first evaluated using the  
500 Monte Carlo simulation experiments adopted by *Xu et al. (2017)* to demonstrate the CQRNN  
501 model. In comparison to MLP, QRNN, and CQRNN models, MCQRNN is more robust than the  
502 benchmark models, especially for non-normal error distributions. Next, the MCQRNN model is  
503 evaluated on real-world climate data by estimating rainfall IDF curves in Canada. Cross-validation  
504 results suggest that the MCQRNN effectively borrows strength across different storm durations  
505 and return periods, which results in a model that is robust against overfitting. In comparison  
506 to standard QRNN, the ability of the MCQRNN model to incorporate monotonicity constraints  
507 – rainfall intensity should increase monotonically as the occurrence frequency and storm duration  
508 decrease – leads to more realistic estimates of extreme rainfall at ungauged sites. While promising,  
509 use of the MCQRNN for IDF curve estimation is presented here as a proof of concept. Other  
510 avenues of research include a more principled consideration of regionalization (*Ouarda et al.,*  
511 *2001*), other covariates (*Madsen et al., 2017*), and comparison against a wider range of nonlinear  
512 methods (*Ouali et al., 2017*). The MCQRNN model architecture is extremely flexible and many  
513 of its features are also not explored in this study. For example, the use of different weights for  
514 each  $\tau$  in the composite QR error function (*Jiang et al., 2012; Sun et al., 2013*), multiple hidden  
515 layers, and the ability to estimate non-crossing, nonlinear expectile regression functions (*Jiang*  
516 *et al., 2017*) are left for future research.

517 Finally, code implementing the MCQRNN model is freely available from the Comprehensive  
518 R Archive Network as part of the `qrnn` package.



## 519 Acknowledgments

520 The author would like to thank Dae Il Jeong, William Hsieh, Dhouha Ouali, and the anonymous re-  
521 viewers for their constructive feedback, and Cuixia Jiang for sharing their CQRNN computer code.  
522 The Comprehensive R Archive Network (CRAN) is acknowledged for hosting the qrnn package  
523 <<https://CRAN.R-project.org/package=qrnn>> for the R programming language and envi-  
524 ronment for statistical computing and graphics.

## 525 Appendix 1: Additive MLP models and control over non-additivity

526 As shown by *Potts* (1999), the MLP architecture used by the MCQRNN model can represent  
527 generalized additive relationships, i.e., where the model output depends on linear combinations of  
528 unknown smooth functions applied to each covariate in turn. Each covariate is associated with its  
529 own MLP, separate from those for the other covariates (Figure 10a), which means that interactions  
530 between covariates are neglected. The resulting model is easy to interpret, as contributions from  
531 covariates can be analyzed in isolation.

532 From Section 2.1 – removing partial monotonicity constraints for sake of simplicity – this is  
533 equivalent to representing the hidden layer outputs in the form

$$h_j(t) = f \left( \sum_{i \in I} x_i(t) A_{ij}^{(h)} W_{ij}^{(h)} + b_j^{(h)} \right) \quad (23)$$

534 where  $\mathbf{A}^{(h)}$  is an appropriate binary mask. For example, for a model with  $\#I = 4$  covariates and  
535  $J = 3(\#I) = 12$  hidden layer outputs, as shown in Figure 10, the mask that enforces additive  
536 relationships is given by

$$\mathbf{A}^{(h)} = \begin{bmatrix} 1 & 1 & 1 & 0 & 0 & 0 & 0 & 0 & 0 & 0 & 0 & 0 \\ 0 & 0 & 0 & 1 & 1 & 1 & 0 & 0 & 0 & 0 & 0 & 0 \\ 0 & 0 & 0 & 0 & 0 & 0 & 1 & 1 & 1 & 0 & 0 & 0 \\ 0 & 0 & 0 & 0 & 0 & 0 & 0 & 0 & 0 & 1 & 1 & 1 \end{bmatrix} \quad (24)$$

537 Each of the covariates  $x_i$  is passed through a smooth function defined, in this example, by a linear  
 538 combination of 3 hidden layer outputs. For a given covariate, the other hidden layer outputs,  
 539 and hence covariates, do not contribute to the output because the additive mask multiplies the  
 540 corresponding elements of  $\mathbf{W}^{(h)}$  by zero (Figure 10b).

541 [Figure 10 about here.]

542 A means of controlling non-additivity in a Gaussian process model was presented by *Plate*  
 543 (1999). It was shown that control over interactions in a flexible nonlinear model – allowing for  
 544 models that range from being fully additive to those that do not constrain covariate interactions –  
 545 can be beneficial for modelling tasks where interpretability and prediction performance are both  
 546 important. Similar fine-grained control can be added to models based on the MLP architecture by  
 547 removing  $\mathbf{A}^{(h)}$  from equation 23 and instead modifying the error function

$$\tilde{E}_\tau^{(A)} = E_\tau^{(A)} + \lambda^{(h)} \frac{1}{VJ} \sum_{i=1}^V \sum_{j=1}^J L_{ij}^{(h)} \left( W_{ij}^{(h)} \right)^2 + \lambda \frac{1}{J} \sum_{j=1}^J (w_j)^2 \quad (25)$$

548 where

$$\mathbf{L}^{(h)} = \begin{bmatrix} 0 & 0 & 0 & 1 & 1 & 1 & 1 & 1 & 1 & 1 & 1 & 1 \\ 1 & 1 & 1 & 0 & 0 & 0 & 1 & 1 & 1 & 1 & 1 & 1 \\ 1 & 1 & 1 & 1 & 1 & 1 & 0 & 0 & 0 & 1 & 1 & 1 \\ 1 & 1 & 1 & 1 & 1 & 1 & 1 & 1 & 1 & 0 & 0 & 0 \end{bmatrix} \quad (26)$$

549 contains the logical negation of elements in the  $\mathbf{A}^{(h)}$  matrix that would be applied in a fully-  
 550 additive model. In effect, the first penalty term now applies only to elements of  $\mathbf{W}^{(h)}$  responsible

551 for controlling interactions between covariates; larger values of  $\lambda^{(h)}$  will therefore suppress non-  
552 additive relationships.

553 To demonstrate, consider MLP models fit using the modified cost function (equation 25) to  
554 synthetic data generated by the function from *Plate* (1999)

$$y = 0.925\phi(x_1, x_2) + 2.248(x_2 + x_3 - 1)^3 + \varepsilon \quad (27)$$

555 where

$$\phi(x_1, x_2) = 1.3356 \left\{ 1.5(1 - x_1) + \exp(2x_1 - 1) \sin \left[ 3\pi(x_1 - 0.6)^2 \right] + \right. \\ \left. \exp[3(x_2 - 0.5)] \sin \left[ 4\pi(x_2 - 0.9)^2 \right] \right\} \quad (28)$$

556 Covariate  $x_1$  has a purely additive and nonlinear relationship with the response, while covariates  
557  $x_2$  and  $x_3$  have an interactive, nonlinear relationship. A fourth covariate  $x_4$ , which is irrelevant and  
558 does not contribute to the response, is also included. Two datasets are created: training data with  
559 300 samples and testing data with 100,000 samples. Each of the four covariates is drawn from a  
560 uniform distribution  $U(0, 1)$  and  $\varepsilon \sim N(0, 0.5)$ .

561 Figure 11 shows generalized additive model plots – modified following *Plate* (1999) so that  
562 non-additive relationships are indicated by vertical spread in points – for MLP models with  $\lambda^{(h)} =$   
563 0, 0.2, 1, 100. Values of  $\lambda^{(h)} = 0, 0.2$  lead to spurious interactions for  $x_1$  and  $x_4$ , whereas  $\lambda^{(h)} =$   
564 100 suppresses the true interactions between  $x_2$  and  $x_3$ .  $\lambda^{(h)} = 1$  appears to strike the appropriate  
565 balance, leading to a MLP model with a nonlinear additive relationship for  $x_1$ , interactions for  $x_2$   
566 and  $x_3$ , and no relationship between  $x_4$  and the response. These results are reflected in the measure  
567 of interaction strength, training and testing RMSE, and magnitudes of  $\mathbf{W}^{(h)}$  elements shown in  
568 Figure 12. The MLP with  $\lambda^{(h)} = 1$  gives the lowest testing RMSE. This model has strong measured  
569 interactions for covariates  $x_2$  and  $x_3$ , which are associated with nonzero elements of  $\mathbf{W}^{(h)}$ .

570 [Figure 11 about here.]

571 [Figure 12 about here.]

## References

- 572
- 573 Alila, Y. (1999), A hierarchical approach for the regionalization of precipitation annual maxima  
574 in Canada, *Journal of Geophysical Research: Atmospheres*, 104(D24), 31,645–31,655, doi:  
575 10.1029/1999JD900764.
- 576 Alila, Y. (2000), Regional rainfall depth-duration-frequency equations for Canada, *Water Re-*  
577 *sources Research*, 36(7), 1767–1778, doi:10.1029/2000WR900046.
- 578 Allamano, P., P. Claps, and F. Laio (2009), Global warming increases flood risk in mountainous  
579 areas, *Geophysical Research Letters*, 36(24), doi:10.1029/2009GL041395.
- 580 Aziz, K., A. Rahman, G. Fang, and S. Shrestha (2014), Application of artificial neural networks in  
581 regional flood frequency analysis: a case study for Australia, *Stochastic Environmental Research*  
582 *and Risk Assessment*, 28(3), 541–554, doi:10.1007/s00477-013-0771-5.
- 583 Baldwin, R. E. (2006), *In Or Out: Does it Matter? An Evidence-based Analysis of the Euro's*  
584 *Trade Effects*, chap. 2, p. 110 pp., Centre for Economic Policy Research (CEPR), London, UK.
- 585 Bang, S., H. Cho, and M. Jhun (2016), Simultaneous estimation for non-crossing multiple quan-  
586 tile regression with right censored data, *Statistics and Computing*, 26(1-2), 131–147, doi:  
587 10.1007/s11222-014-9482-0.
- 588 Barbosa, S. M. (2008), Quantile trends in Baltic sea level, *Geophysical Research Letters*, 35(22),  
589 doi:10.1029/2008GL035182.
- 590 Ben Alaya, M., F. Chebana, and T. Ouarda (2016), Multisite and multivariable statistical downscal-  
591 ing using a Gaussian copula quantile regression model, *Climate Dynamics*, 47(5-6), 1383–1397,  
592 doi:10.1007/s00382-015-2908-3.
- 593 Bondell, H. D., B. J. Reich, and H. Wang (2010), Noncrossing quantile regression curve estimation,  
594 *Biometrika*, 97(4), 825–838, doi:10.1093/biomet/asq048.

595 Burn, D. H. (1990), Evaluation of regional flood frequency analysis with a region of influence  
596 approach, *Water Resources Research*, 26(10), 2257–2265, doi:10.1029/WR026i010p02257.

597 Canadian Standards Association (2012), PLUS 4013 (2nd ed.)–Technical Guide: Development,  
598 Interpretation and Use of Rainfall Intensity-Duration-Frequency (IDF) Information: Guideline  
599 for Canadian Water Resources Practitioners, *Mississauga, Ontario: Canadian Standards Asso-*  
600 *ciation*.

601 Cannon, A. J. (2011), Quantile regression neural networks: Implementation in R and ap-  
602 plication to precipitation downscaling, *Computers & Geosciences*, 37(9), 1277–1284, doi:  
603 10.1016/j.cageo.2010.07.005.

604 Cannon, A. J. (2017), *qrnn: Quantile Regression Neural Network*, R package version 2.0.2.

605 Cawley, G. C., G. J. Janacek, M. R. Haylock, and S. R. Dorling (2007), Predictive uncertainty in  
606 environmental modelling, *Neural Networks*, 20(4), 537–549, doi:10.1016/j.neunet.2007.04.024.

607 Chen, C. (2007), A finite smoothing algorithm for quantile regression, *Journal of Computational*  
608 *and Graphical Statistics*, 16(1), 136–164, doi:10.1198/106186007X180336.

609 Chernozhukov, V., I. Fernández-Val, and A. Galichon (2010), Quantile and probability curves  
610 without crossing, *Econometrica*, 78(3), 1093–1125, doi:10.3982/ECTA7880.

611 Doksum, K., and J.-Y. Koo (2000), On spline estimators and prediction intervals in nonparamet-  
612 ric regression, *Computational Statistics & Data Analysis*, 35(1), 67–82, doi:10.1016/S0167-  
613 9473(99)00116-4.

614 Environment and Climate Change Canada (2014), *Intensity-Duration-Frequency (IDF) Files*  
615 *v2.30*.

616 Friederichs, P., and A. Hense (2007), Statistical downscaling of extreme precipitation events  
617 using censored quantile regression, *Monthly Weather Review*, 135(6), 2365–2378, doi:  
618 10.1175/MWR3403.1.

619 Hanson, S. J., and D. J. Burr (1988), Minkowski-r back-propagation: Learning in connectionist  
620 models with non-Euclidian error signals, in *Neural Information Processing Systems*, pp. 348–  
621 357.

622 Hirschi, M., S. I. Seneviratne, V. Alexandrov, F. Boberg, C. Boroneant, O. B. Christensen,  
623 H. Formayer, B. Orlowsky, and P. Stepanek (2010), Observational evidence for soil-moisture  
624 impact on hot extremes in southeastern Europe, *Nature Geoscience*, 4(1), ngeo1032, doi:  
625 10.1038/ngeo1032.

626 Hofmeister, T. (2017), *qrsvm: SVM Quantile Regression with the Pinball Loss*, R package version  
627 0.2.1.

628 Huber, P. J. (1964), Robust estimation of a location parameter, *The Annals of Mathematical Statis-*  
629 *tics*, 35(1), 73–101.

630 Jiang, C., M. Jiang, Q. Xu, and X. Huang (2017), Expectile regression neural network model with  
631 applications, *Neurocomputing*, 247, 73–86, doi:10.1016/j.neucom.2017.03.040.

632 Jiang, X., J. Jiang, and X. Song (2012), Oracle model selection for nonlinear models  
633 based on weighted composite quantile regression, *Statistica Sinica*, pp. 1479–1506, doi:  
634 10.5705/ss.2010.203.

635 Karatzoglou, A., A. Smola, K. Hornik, and A. Zeileis (2004), kernlab – an S4 package for kernel  
636 methods in R, *Journal of Statistical Software*, 11(9), 1–20.

637 Koenker, R., and G. Bassett Jr. (1978), Regression quantiles, *Econometrica: Journal of the Econo-*  
638 *metric Society*, pp. 33–50.

639 Koenker, R., and F. Schorfheide (1994), Quantile spline models for global temperature change,  
640 *Climatic Change*, 28(4), 395–404, doi:10.1007/BF01104081.

641 Kuo, C.-C., T. Y. Gan, and S. Chan (2012), Regional intensity-duration-frequency curves derived

642 from ensemble empirical mode decomposition and scaling property, *Journal of Hydrologic En-*  
643 *gineering*, 18(1), 66–74, doi:10.1061/(ASCE)HE.1943-5584.0000612.

644 Lang, B. (2005), Monotonic multi-layer perceptron networks as universal approximators, *Artifi-*  
645 *cial Neural Networks: Formal Models and Their Applications–ICANN 2005*, pp. 31–37, doi:  
646 10.1007/11550907\_6.

647 Liu, Y., and Y. Wu (2009), Stepwise multiple quantile regression estimation using non-crossing  
648 constraints, *Statistics and its Interface*, 2(3), 299–310, doi:10.4310/SII.2009.v2.n3.a4.

649 Liu, Y., and Y. Wu (2011), Simultaneous multiple non-crossing quantile regression estima-  
650 tion using kernel constraints, *Journal of Nonparametric Statistics*, 23(2), 415–437, doi:  
651 10.1080/10485252.2010.537336.

652 Madsen, H., I. B. Gregersen, D. Rosbjerg, and K. Arnbjerg-Nielsen (2017), Regional frequency  
653 analysis of short duration rainfall extremes using gridded daily rainfall data as co-variate, *Water*  
654 *Science and Technology*, 75(8), 1971–1981, doi:10.2166/wst.2017.089.

655 Mailhot, A., S. Lachance-Cloutier, G. Talbot, and A.-C. Favre (2013), Regional estimates of in-  
656 tense rainfall based on the Peak-Over-Threshold (POT) approach, *Journal of Hydrology*, 476,  
657 188–199, doi:10.1016/j.jhydrol.2012.10.036.

658 McKenney, D. W., M. F. Hutchinson, P. Papadopol, K. Lawrence, J. Pedlar, K. Campbell,  
659 E. Milewska, R. F. Hopkinson, D. Price, and T. Owen (2011), Customized spatial climate mod-  
660 els for North America, *Bulletin of the American Meteorological Society*, 92(12), 1611–1622,  
661 doi:10.1175/2011BAMS3132.1.

662 Minin, A., M. Velikova, B. Lang, and H. Daniels (2010), Comparison of universal approxima-  
663 tors incorporating partial monotonicity by structure, *Neural Networks*, 23(4), 471–475, doi:  
664 10.1016/j.neunet.2009.09.002.

665 Mishra, V., F. Dominguez, and D. P. Lettenmaier (2012), Urban precipitation extremes: How  
666 reliable are regional climate models?, *Geophysical Research Letters*, 39, L03,407, doi:  
667 10.1029/2011GL050658.

668 Muggeo, V. M., M. Sciandra, and L. Augugliaro (2012), Quantile regression via iterative least  
669 squares computations, *Journal of Statistical Computation and Simulation*, 82(11), 1557–1569,  
670 doi:10.1080/00949655.2011.583650.

671 Muggeo, V. M., M. Sciandra, A. Tomasello, and S. Calvo (2013), Estimating growth charts via  
672 nonparametric quantile regression: a practical framework with application in ecology, *Environ-  
673 mental and Ecological Statistics*, 20(4), 519–531, doi:10.1007/s10651-012-0232-1.

674 Newey, W. K., and J. L. Powell (1987), Asymmetric least squares estimation and testing, *Econo-  
675 metrica*, pp. 819–847.

676 Ouali, D., and A. J. Cannon (2017), Estimation of rainfall Intensity-Duration-Frequency curves at  
677 ungauged locations using quantile regression methods, *Stochastic Environmental Research and  
678 Risk Assessment*.

679 Ouali, D., F. Chebana, and T. Ouarda (2016), Quantile regression in regional frequency analysis:  
680 A better exploitation of the available information, *Journal of Hydrometeorology*, 17(6), 1869–  
681 1883, doi:10.1175/JHM-D-15-0187.1.

682 Ouali, D., F. Chebana, and T. Ouarda (2017), Fully nonlinear statistical and machine-learning  
683 approaches for hydrological frequency estimation at ungauged sites, *Journal of Advances in  
684 Modeling Earth Systems*, 9(2), 1292–1306, doi:10.1002/2016MS000830.

685 Ouarda, T. B., C. Girard, G. S. Cavadias, and B. Bobée (2001), Regional flood frequency estimation  
686 with canonical correlation analysis, *Journal of Hydrology*, 254(1), 157–173, doi:10.1016/S0022-  
687 1694(01)00488-7.



- 688 Persson, T. (2001), Currency unions and trade: how large is the treatment effect?, *Economic Policy*,  
689 33, 435–448.
- 690 Plate, T. A. (1999), Accuracy versus interpretability in flexible modeling: Implementing a tradeoff  
691 using Gaussian process models, *Behaviormetrika*, 26(1), 29–50.
- 692 Potts, W. J. (1999), Generalized additive neural networks, in *Proceedings of the Fifth ACM*  
693 *SIGKDD International Conference on Knowledge Discovery and Data Mining*, pp. 194–200,  
694 ACM.
- 695 Quiñonero Candela, J., C. E. Rasmussen, F. Sinz, O. Bousquet, and B. Schölkopf (2006), Eval-  
696 uating predictive uncertainty challenge, *Lecture Notes in Computer Science*, 3944, 1–27, doi:  
697 10.1007/11736790\_1.
- 698 Roth, M., T. Buishand, and G. Jongbloed (2015), Trends in moderate rainfall extremes: A regional  
699 monotone regression approach, *Journal of Climate*, 28(22), 8760–8769, doi:10.1175/JCLI-D-  
700 14-00685.1.
- 701 Saito, H., D. Nakayama, and H. Matsuyama (2010), Relationship between the initiation of a shal-  
702 low landslide and rainfall intensity-duration thresholds in Japan, *Geomorphology*, 118(1), 167–  
703 175, doi:10.1016/j.geomorph.2009.12.016.
- 704 Shephard, M. W., E. Mekis, R. J. Morris, Y. Feng, X. Zhang, K. Kilcup, and R. Fleetwood (2014),  
705 Trends in Canadian short-duration extreme rainfall: Including an Intensity–Duration–Frequency  
706 perspective, *Atmosphere-Ocean*, 52(5), 398–417, doi:10.1080/07055900.2014.969677.
- 707 Sun, J., Y. Gai, and L. Lin (2013), Weighted local linear composite quantile estimation for the case  
708 of general error distributions, *Journal of Statistical Planning and Inference*, 143(6), 1049–1063,  
709 doi:10.1016/j.jspi.2013.01.002.
- 710 Takeuchi, I., Q. V. Le, T. D. Sears, and A. J. Smola (2006), Nonparametric quantile estimation,  
711 *Journal of Machine Learning Research*, 7(Jul), 1231–1264.

- 712 Taylor, J. W. (2000), A quantile regression neural network approach to estimating the condi-  
713 tional density of multiperiod returns, *Journal of Forecasting*, 19(4), 299–311, doi:10.1002/1099-  
714 131X(200007)19:4<299::AID-FOR775>3.0.CO;2-V.
- 715 Waltrup, L. S., F. Sobotka, T. Kneib, and G. Kauermann (2015), Expectile and quantile regression–  
716 David and Goliath?, *Statistical Modelling*, 15(5), 433–456, doi:10.1177/1471082X14561155.
- 717 Wasko, C., and A. Sharma (2014), Quantile regression for investigating scaling of ex-  
718 treme precipitation with temperature, *Water Resources Research*, 50(4), 3608–3614, doi:  
719 10.1002/2013WR015194.
- 720 White, H. (1992), Nonparametric estimation of conditional quantiles using neural networks, in  
721 *Computing Science and Statistics*, edited by C. Page and R. LePage, pp. 190–199, Springer,  
722 doi:10.1007/978-1-4612-2856-1\_25.
- 723 Xu, Q., K. Deng, C. Jiang, F. Sun, and X. Huang (2017), Composite quantile regression  
724 neural network with applications, *Expert Systems with Applications*, 76, 129–139, doi:  
725 10.1016/j.eswa.2017.01.054.
- 726 Yao, Q., and H. Tong (1996), Asymmetric least squares regression estimation: A  
727 nonparametric approach, *Journal of Nonparametric Statistics*, 6(2-3), 273–292, doi:  
728 10.1080/10485259608832675.
- 729 Zhang, H., and Z. Zhang (1999), Feedforward networks with monotone constraints, in *IJCNN'99*,  
730 *International Joint Conference on Neural Networks*, vol. 3, pp. 1820–1823, IEEE, doi:  
731 10.1109/IJCNN.1999.832655.
- 732 Zou, H., and M. Yuan (2008), Composite quantile regression and the oracle model selection theory,  
733 *The Annals of Statistics*, pp. 1108–1126, doi:10.1214/07-AOS507.

734 **List of Figures**

735 1 Predictions from QRNN (panels a and c) and MCQRNN (panels b and d) models  
736 fit to synthetic data (black points) generated by equation 15 (panels a and b) and  
737 equation 16 (panels c and d) are shown in rainbow colours. Plots of the true con-  
738 ditional quantile functions are shown by solid grey lines. The nine curves from  
739 bottom to top represent  $\tau = 0.1, 0.2, \dots, 0.9$ . . . . . 37

740 2 As in Figures 1b and 1d, but for MCQRNN models with additional (a) positivity  
741 constraints and (b) positivity and monotonicity constraints, respectively. (c, d)  
742 Estimates of 95% confidence intervals, based on 500 parametric bootstrap datasets,  
743 for the  $\tau = 0.1, 0.5, 0.9$ -quantile regression curves shown in Figures 1b and 1d. . . 38

744 3 Predictions from (a) CQRNN, CQRNN\*, and (b) MCQRNN models on the exam-  
745 ple 2 dataset (equation 18) with  $\varepsilon \sim \chi^2(3)$  distributed noise. Black dots show the  
746 synthetic training data and the thick black line indicates the true underlying func-  
747 tion. Predictions of the conditional mean by CQRNN, CQRNN\*, and MCQRNN  
748 are shown by the blue line in (a), the red line in (a), and the red line in (b), re-  
749 spectively. For the CQRNN\* and MCQRNN models, these values are obtained by  
750 taking the mean over predictions of the  $K = 19$   $\tau$ -quantiles shown in grey. Places  
751 where CQRNN\* quantiles cross are indicated by vertical grey dashed lines. . . . . 39

752 4 Distribution of RMSE values over the 1000 Monte Carlo simulations for MLP  
753 (black), QRNN (green), CQRNN (blue), CQRNN\* (orange) and MCQRNN (red)  
754 models in the (a) training and (b) testing datasets for examples 1, 2, and 3 from *Xu*  
755 *et al.* (2017) with  $N(0, 0.25)$  (rnorm25),  $t(3)$  (rt3), and  $\chi^2(3)$  (rchisq3) distributed  
756 noise. The central dot indicates the median RMSE and the lower and upper bars  
757 the 5th and 95th percentiles, respectively. . . . . 40

758 5 Points (●) show locations of ECCC IDF curve stations; point size is proportional to  
759 station elevation. Shading indicates the climatological summer total precipitation  
760 (1971-2000). . . . . 41

761 6 Example ECCC IDF data for Victoria Intl A (station 1018621) in British Columbia,  
762 Canada. Points (×) show quantiles associated with 2-yr, 5-yr, 10-yr, 25-yr, 50-yr,  
763 and 100-yr (from bottom to top) return period intensities estimated by fitting the  
764 Gumbel distribution by the method of moments to annual maximum rainfall rate  
765 data for 5-, 10-, 15-, 30-, 60-min, 2-, 6-, 12-, and 24-hr durations (left to right).  
766 Lines are from best fit linear interpolation equations between log-transformed du-  
767 ration and log-transformed Gumbel quantiles for each return period. . . . . 42

768 7 Leave-one-out predictions of IDF curves for 2-yr, 5-yr, 10-yr, 25-yr, 50-yr, and  
769 100-yr (in rainbow colours from bottom to top) return period intensities for Victo-  
770 ria Intl A (station 1018621) from (a) QRNN models and (b) MCQRNN model (cf.  
771 Figure 6). Points (■) show observed annual maximum rainfall rate data for 5-, 10-,  
772 15-, 30-, 60-min, 2-, 6-, 12-, and 24-hr durations. . . . . 43

773 8 Cross-validated relative differences  $RD_\tau$  (%) in quantile regression error between  
774 MCQRNN and QRNN IDF curve predictions for  $J = 1, 2, \dots, 5$  using QRNN ( $J =$   
775  $1$ ) as the reference model. Results are shown for 2-yr, 5-yr, 10-yr, 25-yr, 50-yr, and  
776 100-yr return periods. . . . . 44

777	9	Mean quantile regression error ratio $R_\tau$ between at-site ECCC IDF curves and leave-one-out cross-validated MCQRNN predictions; values of $R_\tau$ are stratified according to the median distance between the left-out station and its 80 neighbouring stations. Each of the 10 distance groupings contains an approximately equal numbers of stations (56 or 57). . . . .	45
778			
779			
780			
781			
782	10	Schematic representations of (a) the generalized additive neural network architecture from <i>Potts</i> (1999) and (b) additivity constraints applied to a fully-connected MLP via a binary mask $\mathbf{A}^{(h)}$ applied to elements of $\mathbf{W}^{(h)}$ . Parameters that have been set to zero by $\mathbf{A}^{(h)}$ are represented by dashed grey lines. Nonzero $\mathbf{W}^{(h)}$ , $\mathbf{w}$ parameters are represented by solid coloured lines, $\mathbf{b}^{(h)}$ parameters by dashed coloured lines, and $b$ by dashed black lines. . . . .	46
783			
784			
785			
786			
787			
788	11	Modified generalized additive model plots ( <i>Plate</i> , 1999) shows partial effects for covariates $x_1$ , $x_2$ , $x_3$ , and $x_4$ from MLP models ( $\lambda^{(h)} = 0, 0.2, 1, 100$ ) fit to synthetic data generated by equation 27. . . . .	47
789			
790			
791	12	(a) Interaction strength for covariates $x_1$ , $x_2$ , $x_3$ , and $x_4$ ( <i>Plate</i> , 1999), (b) training and testing RMSE, and (c) absolute magnitudes of $\mathbf{W}^{(h)}$ elements (cf. equation 26) associated with different values of $\lambda^{(h)}$ . . . . .	48
792			
793			

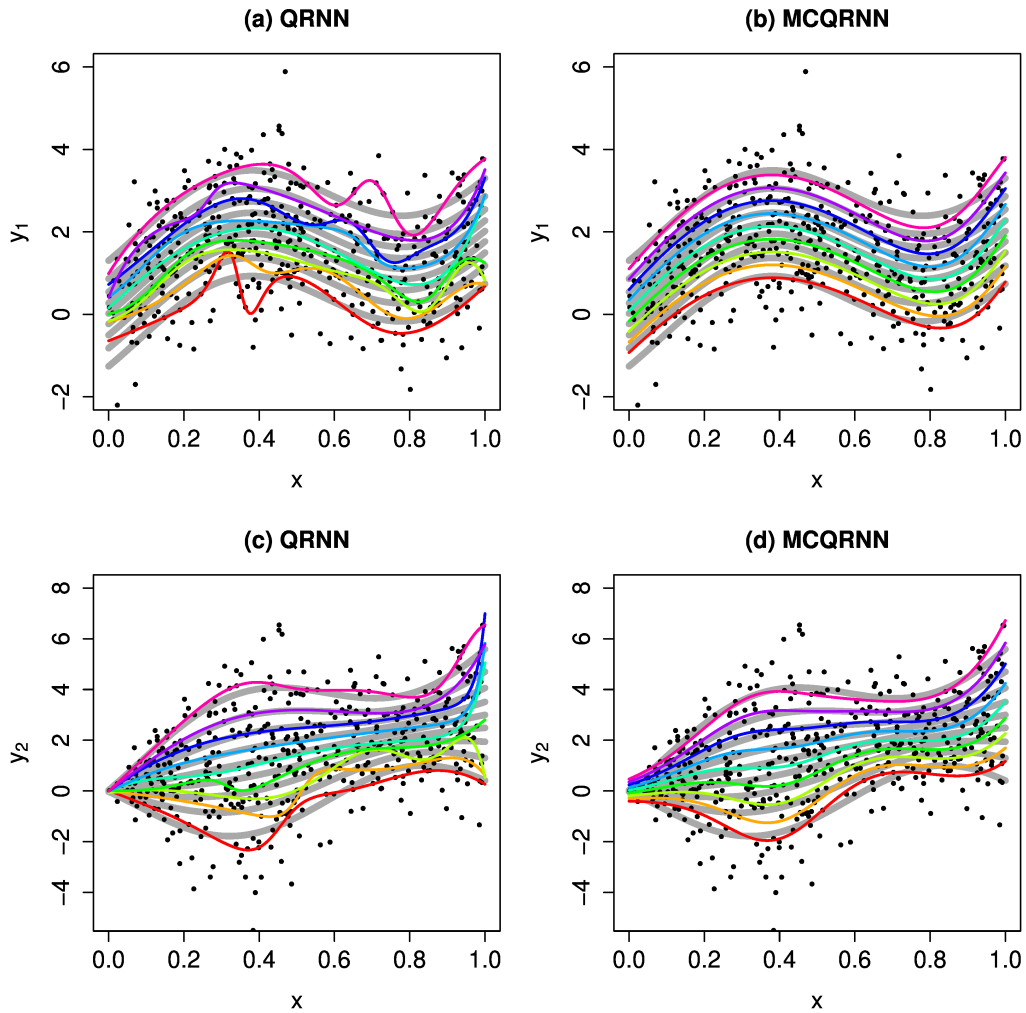


Figure 1: Predictions from QRNN (panels a and c) and MCQRNN (panels b and d) models fit to synthetic data (black points) generated by equation 15 (panels a and b) and equation 16 (panels c and d) are shown in rainbow colours. Plots of the true conditional quantile functions are shown by solid grey lines. The nine curves from bottom to top represent  $\tau = 0.1, 0.2, \dots, 0.9$ .

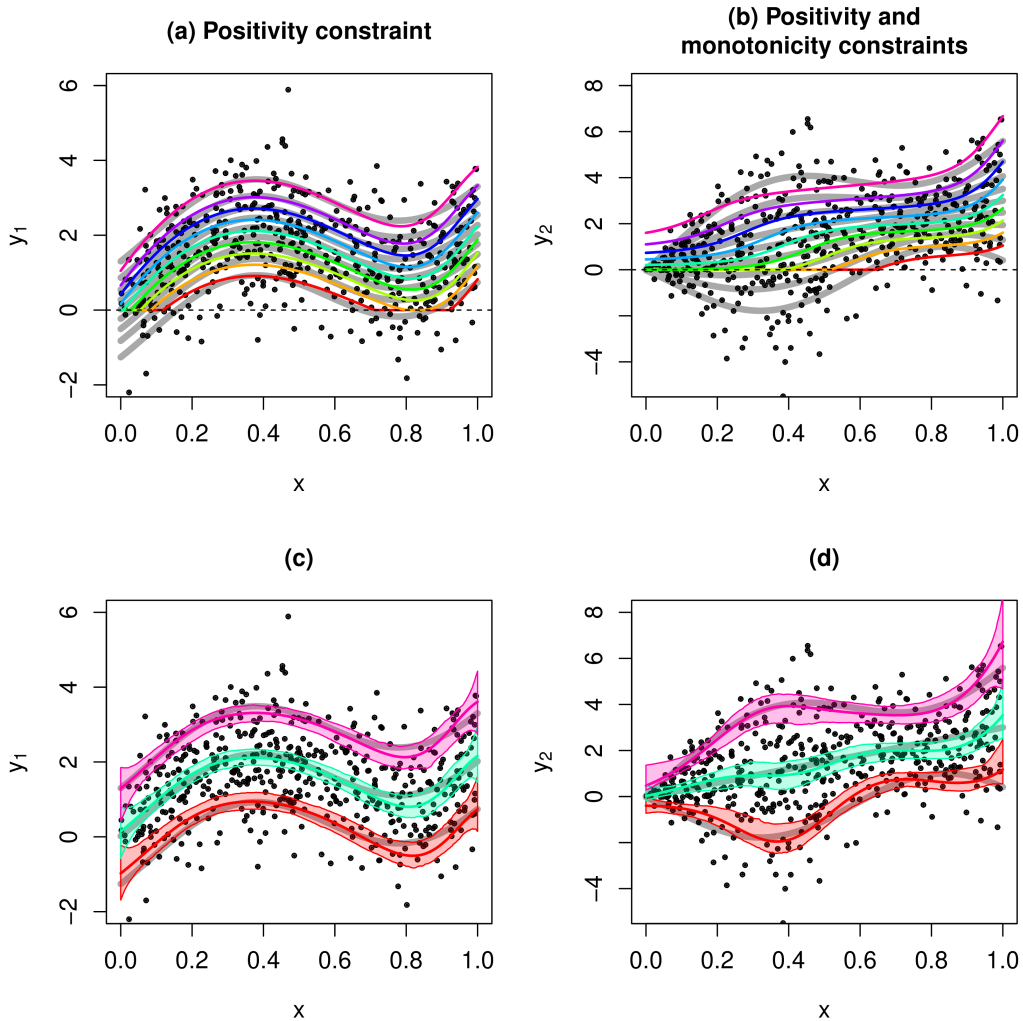


Figure 2: As in Figures 1b and 1d, but for MCQRNN models with additional (a) positivity constraints and (b) positivity and monotonicity constraints, respectively. (c, d) Estimates of 95% confidence intervals, based on 500 parametric bootstrap datasets, for the  $\tau = 0.1, 0.5, 0.9$ -quantile regression curves shown in Figures 1b and 1d.

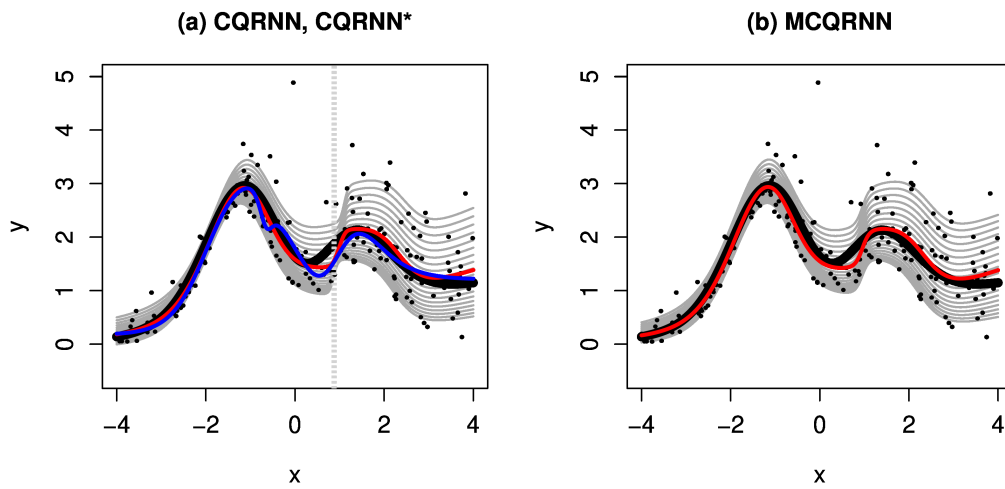


Figure 3: Predictions from (a) CQRNN, CQRNN\*, and (b) MCQRNN models on the example 2 dataset (equation 18) with  $\varepsilon \sim \chi^2(3)$  distributed noise. Black dots show the synthetic training data and the thick black line indicates the true underlying function. Predictions of the conditional mean by CQRNN, CQRNN\*, and MCQRNN are shown by the blue line in (a), the red line in (a), and the red line in (b), respectively. For the CQRNN\* and MCQRNN models, these values are obtained by taking the mean over predictions of the  $K = 19$   $\tau$ -quantiles shown in grey. Places where CQRNN\* quantiles cross are indicated by vertical grey dashed lines.

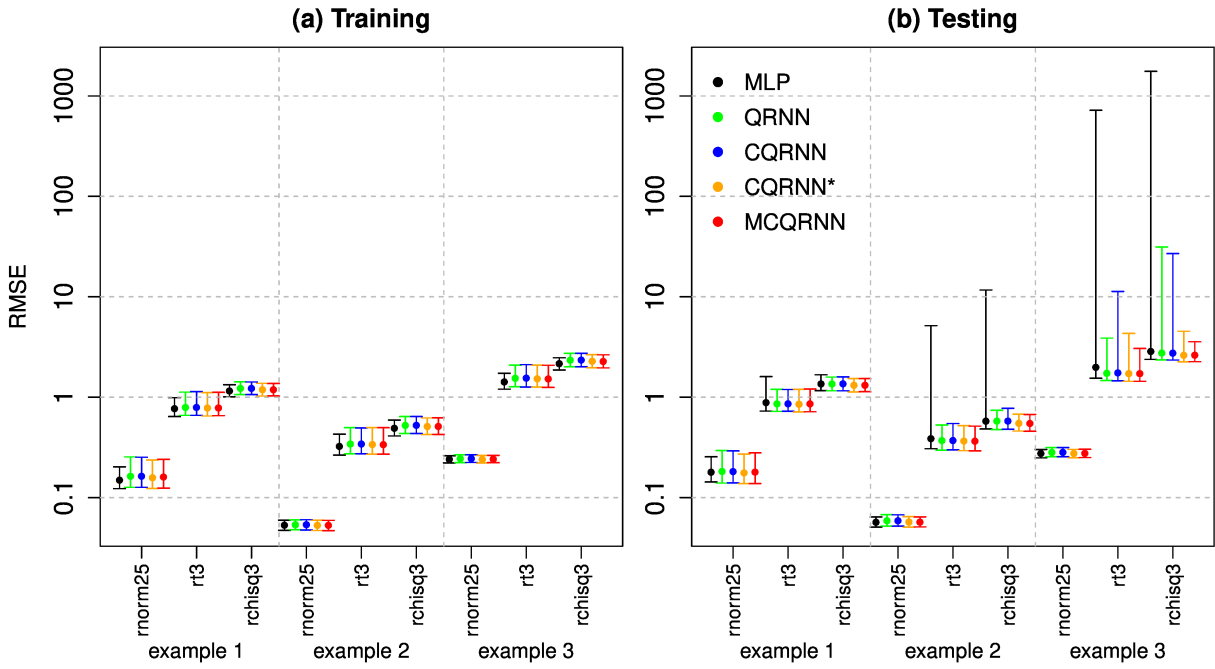


Figure 4: Distribution of RMSE values over the 1000 Monte Carlo simulations for MLP (black), QRNN (green), CQRNN (blue), CQRNN\* (orange) and MCQRNN (red) models in the (a) training and (b) testing datasets for examples 1, 2, and 3 from *Xu et al. (2017)* with  $N(0, 0.25)$  (rnorm25),  $t(3)$  (rt3), and  $\chi^2(3)$  (rchisq3) distributed noise. The central dot indicates the median RMSE and the lower and upper bars the 5th and 95th percentiles, respectively.



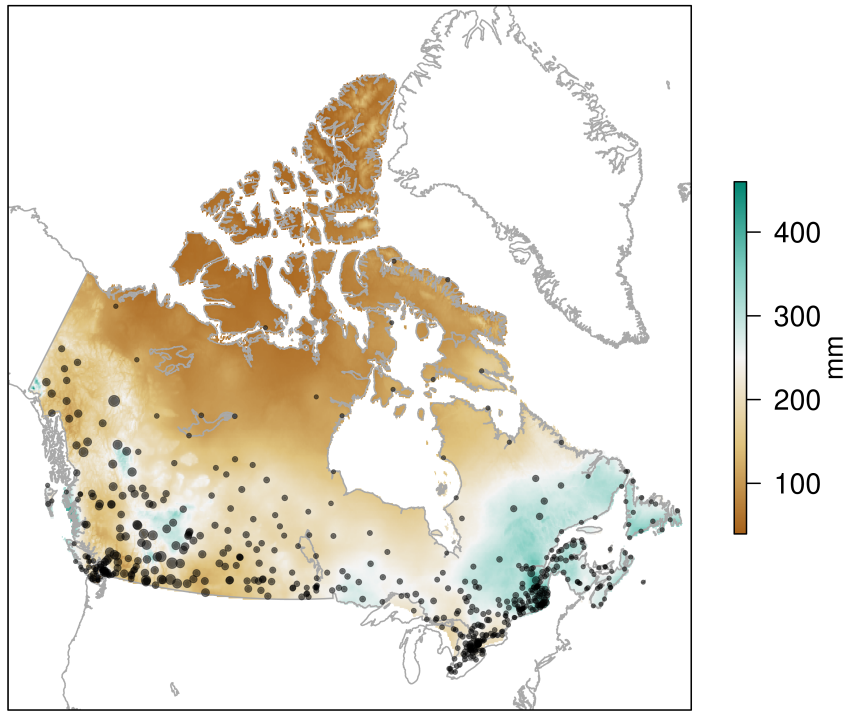


Figure 5: Points (●) show locations of ECCC IDF curve stations; point size is proportional to station elevation. Shading indicates the climatological summer total precipitation (1971-2000).

### Short Duration Rainfall Intensity–Duration–Frequency Data

2014/12/21

### Données sur l'intensité, la durée et la fréquence des chutes de pluie de courte durée

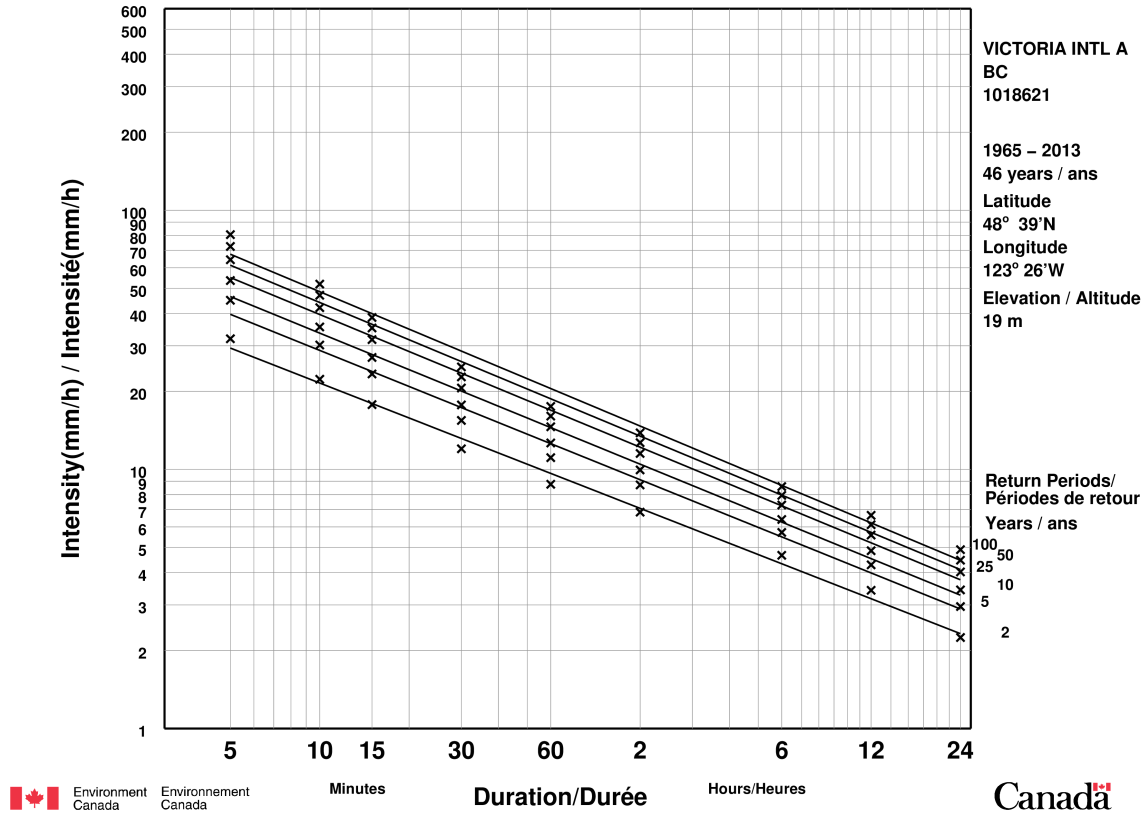


Figure 6: Example ECCC IDF data for Victoria Intl A (station 1018621) in British Columbia, Canada. Points (×) show quantiles associated with 2-yr, 5-yr, 10-yr, 25-yr, 50-yr, and 100-yr (from bottom to top) return period intensities estimated by fitting the Gumbel distribution by the method of moments to annual maximum rainfall rate data for 5-, 10-, 15-, 30-, 60-min, 2-, 6-, 12-, and 24-hr durations (left to right). Lines are from best fit linear interpolation equations between log-transformed duration and log-transformed Gumbel quantiles for each return period.

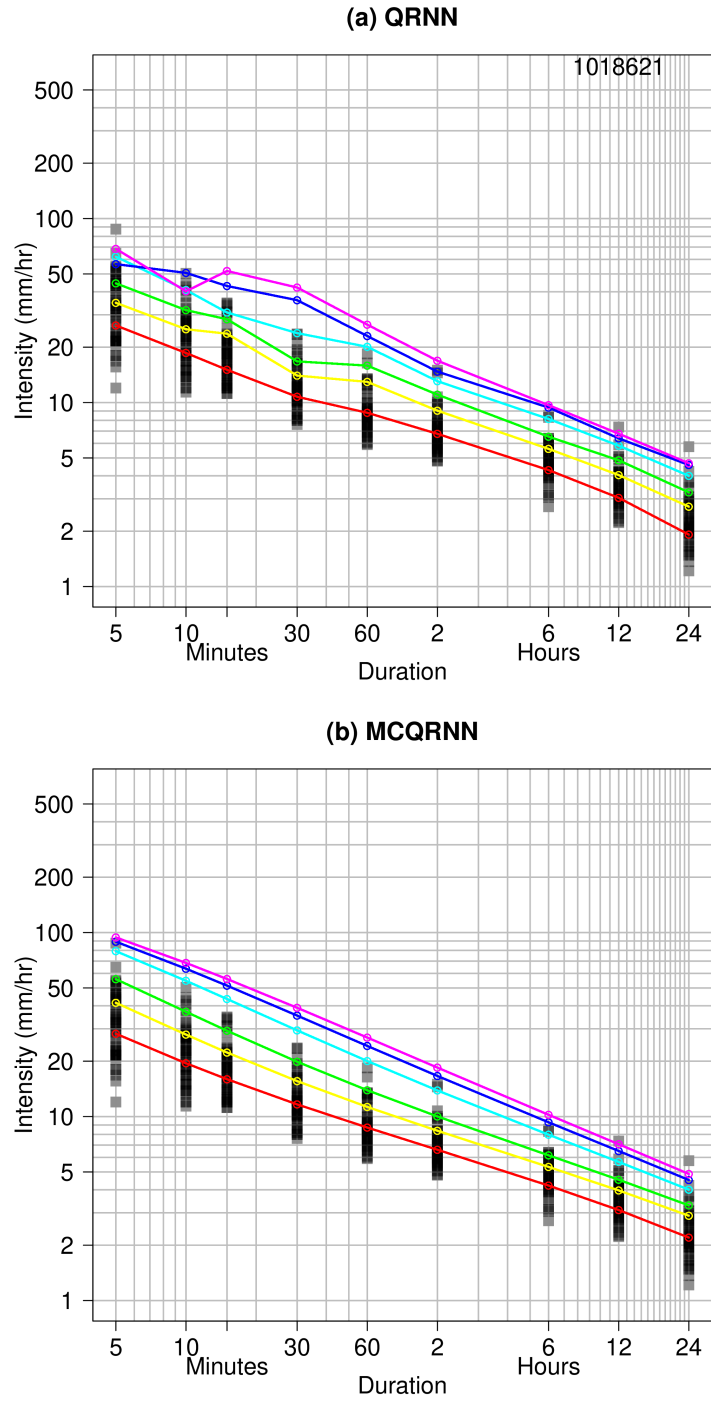


Figure 7: Leave-one-out predictions of IDF curves for 2-yr, 5-yr, 10-yr, 25-yr, 50-yr, and 100-yr (in rainbow colours from bottom to top) return period intensities for Victoria Intl A (station 1018621) from (a) QRNN models and (b) MCQRNN model (cf. Figure 6). Points (■) show observed annual maximum rainfall rate data for 5-, 10-, 15-, 30-, 60-min, 2-, 6-, 12-, and 24-hr durations.

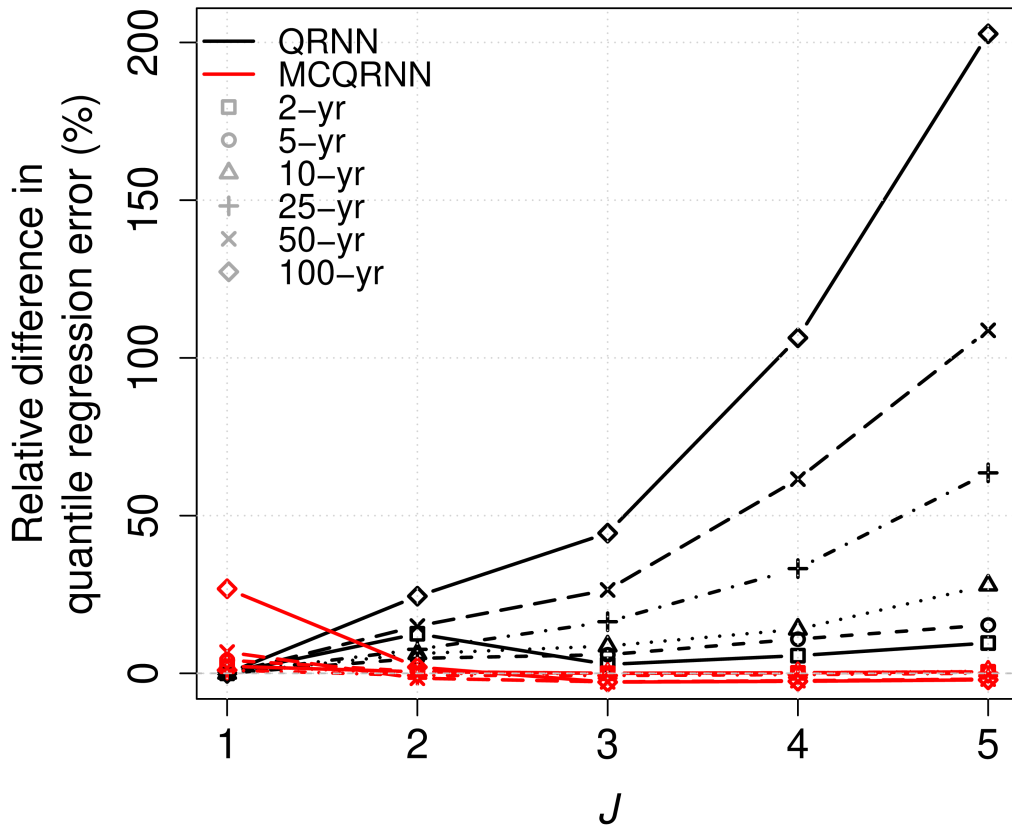


Figure 8: Cross-validated relative differences  $RD_{\tau}$  (%) in quantile regression error between MCQRNN and QRNN IDF curve predictions for  $J = 1, 2, \dots, 5$  using QRNN ( $J = 1$ ) as the reference model. Results are shown for 2-yr, 5-yr, 10-yr, 25-yr, 50-yr, and 100-yr return periods.

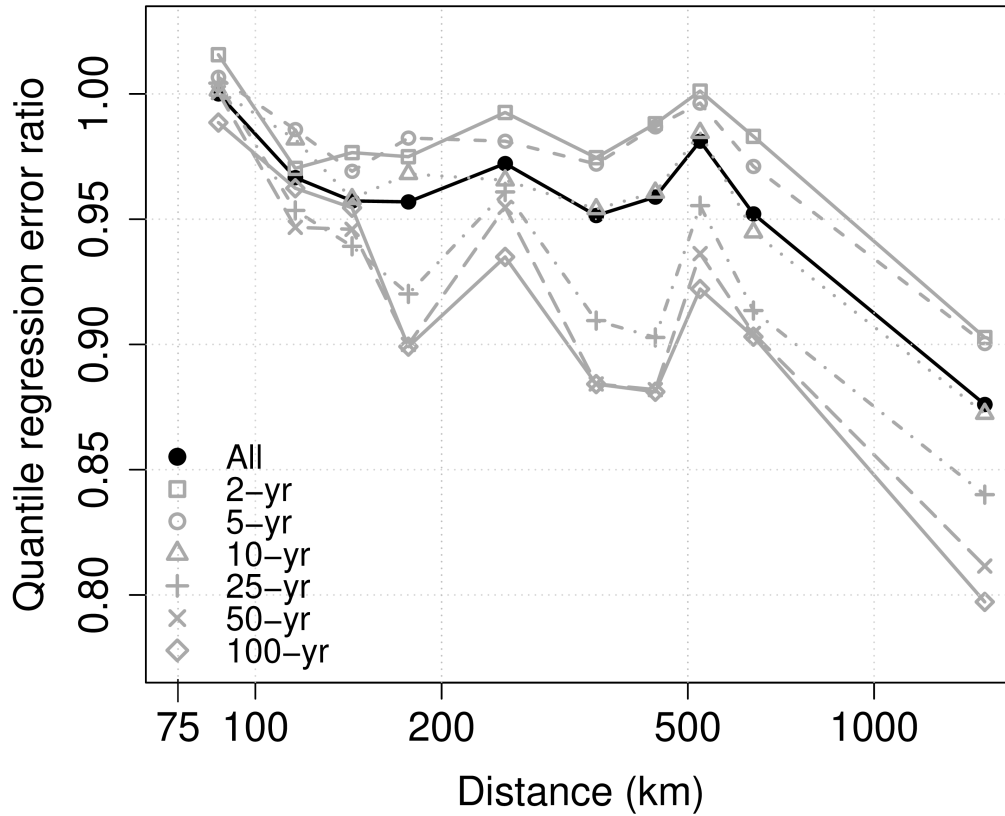


Figure 9: Mean quantile regression error ratio  $R_\tau$  between at-site ECCC IDF curves and leave-one-out cross-validated MCQRNN predictions; values of  $R_\tau$  are stratified according to the median distance between the left-out station and its 80 neighbouring stations. Each of the 10 distance groupings contains an approximately equal numbers of stations (56 or 57).

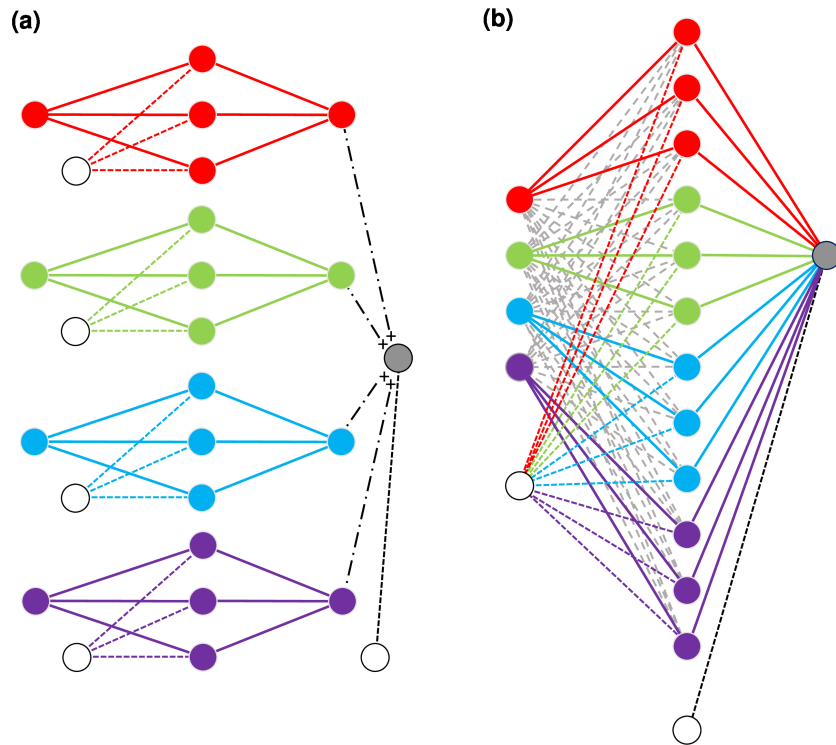


Figure 10: Schematic representations of (a) the generalized additive neural network architecture from *Potts* (1999) and (b) additivity constraints applied to a fully-connected MLP via a binary mask  $\mathbf{A}^{(h)}$  applied to elements of  $\mathbf{W}^{(h)}$ . Parameters that have been set to zero by  $\mathbf{A}^{(h)}$  are represented by dashed grey lines. Nonzero  $\mathbf{W}^{(h)}$ ,  $\mathbf{w}$  parameters are represented by solid coloured lines,  $\mathbf{b}^{(h)}$  parameters by dashed coloured lines, and  $b$  by dashed black lines.

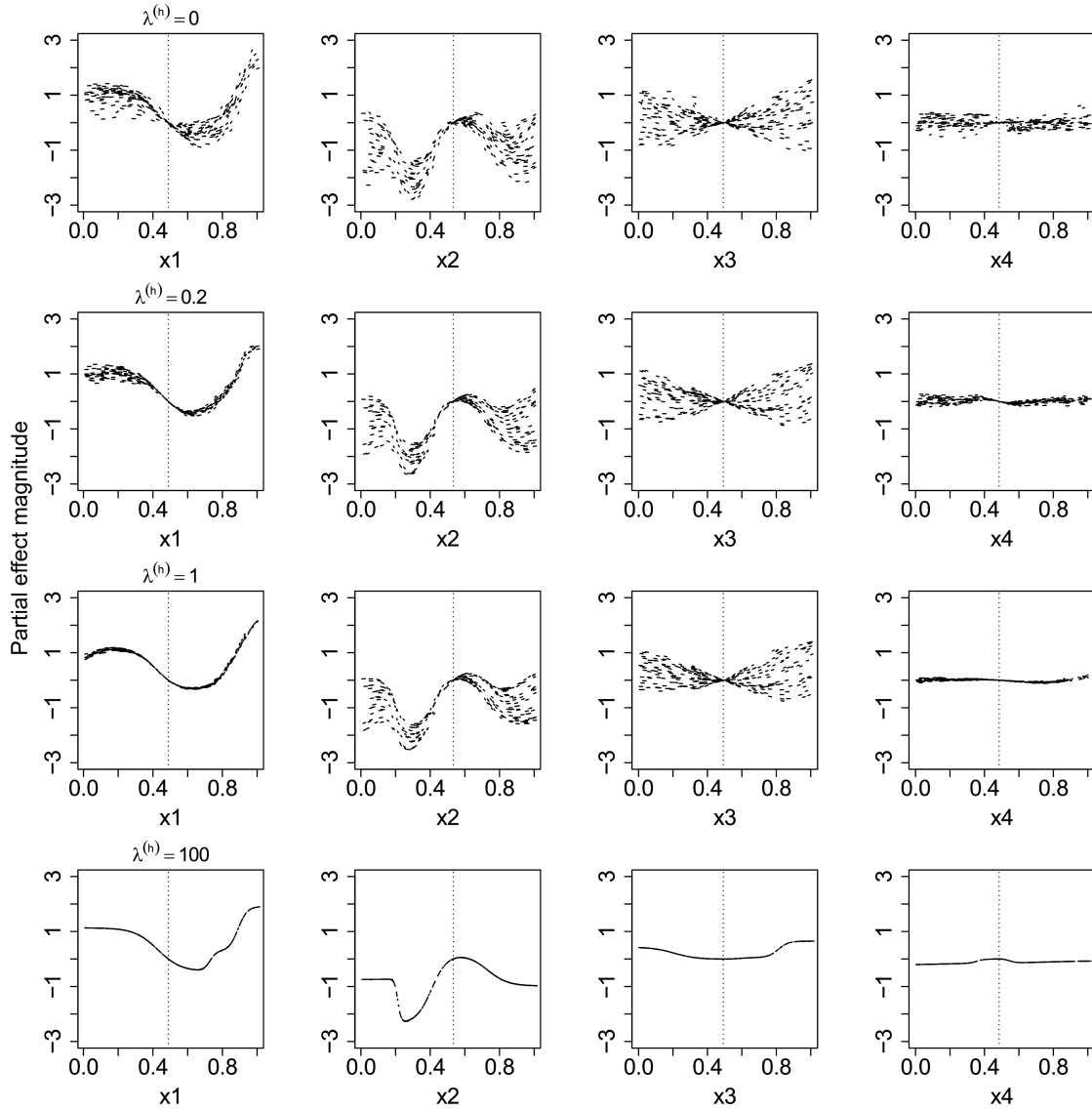


Figure 11: Modified generalized additive model plots (*Plate, 1999*) shows partial effects for covariates  $x_1$ ,  $x_2$ ,  $x_3$ , and  $x_4$  from MLP models ( $\lambda^{(h)} = 0, 0.2, 1, 100$ ) fit to synthetic data generated by equation 27.

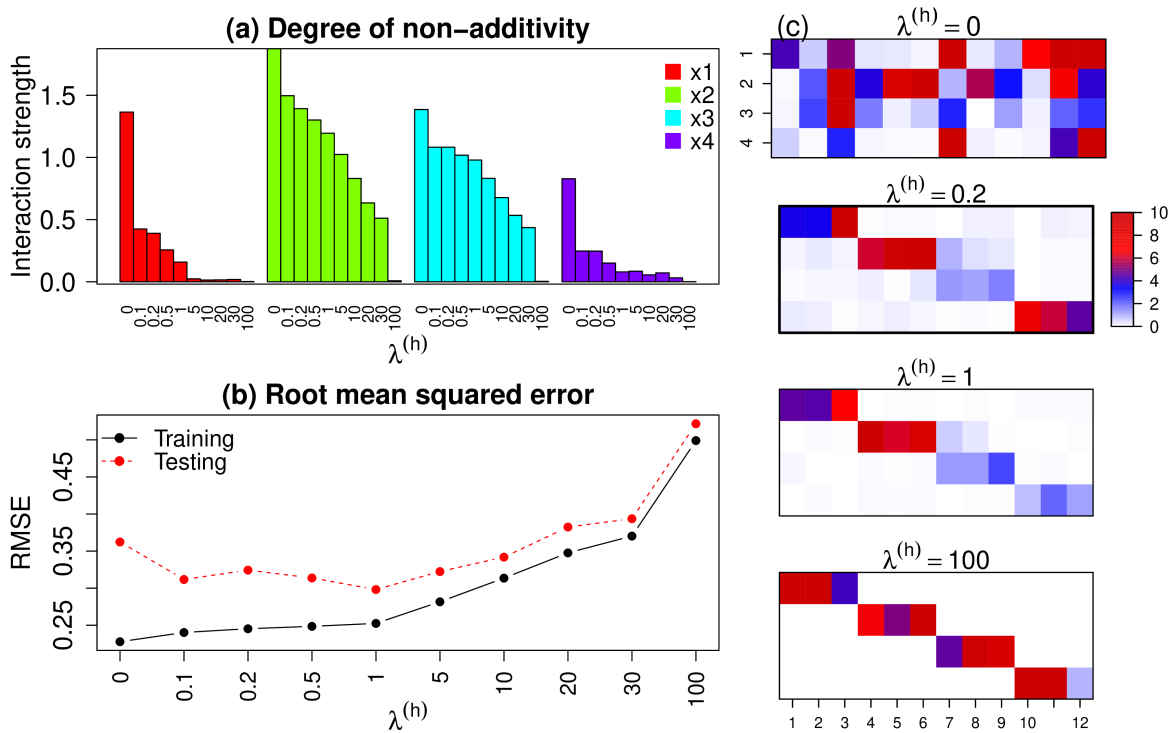


Figure 12: (a) Interaction strength for covariates  $x_1$ ,  $x_2$ ,  $x_3$ , and  $x_4$  (Plate, 1999), (b) training and testing RMSE, and (c) absolute magnitudes of  $\mathbf{W}^{(h)}$  elements (cf. equation 26) associated with different values of  $\lambda^{(h)}$ .



794 **List of Tables**

795 1 Summary of cross-validated relative differences  $RD_{\tau}$  (%) in quantile regression  
796 error stratified by duration  $D$ , for all stations, for MCQRNN models (a) without  
797 weighting and (b) with weighting proportional to  $\log(D)$ . In both cases, QRNN  
798 IDF curve predictions serve as the reference model. Bold values indicate combi-  
799 nations of return period and duration for which MCQRNN performs better (i.e.,  
800 lower errors) than QRNN; combinations with worse performance are underlined. . 50

801 2 Summary of quantile regression error ratio  $R_{\tau}$  stratified by duration  $D$  between at-  
802 site ECCC IDF curves and ungauged MCQRNN predictions for all stations. Values  
803  $\geq 0.9$  are shown in bold. . . . . 51

Table 1: Summary of cross-validated relative differences  $RD_\tau$  (%) in quantile regression error stratified by duration  $D$ , for all stations, for MCQRNN models (a) without weighting and (b) with weighting proportional to  $\log(D)$ . In both cases, QRNN IDF curve predictions serve as the reference model. Bold values indicate combinations of return period and duration for which MCQRNN performs better (i.e., lower errors) than QRNN; combinations with worse performance are underlined.

(a) Unweighted

Return period / Duration	5-min	10-min	15-min	30-min	60-min	2-hr	6-hr	12-hr	24-hr
2	<b>-0.1</b>	<b>-0.2</b>	0	<u>+0.1</u>	<b>-0.1</b>	<u>+0.4</u>	<u>+1.5</u>	<u>+2.7</u>	<u>+4.8</u>
5	<b>-0.1</b>	<u>+0.2</u>	<u>+0.3</u>	<b>-0.6</b>	<b>-0.4</b>	<b>-0.3</b>	<u>+1.0</u>	<u>+0.5</u>	<u>+1.9</u>
10	<u>+0.2</u>	<u>+0.1</u>	<u>+0.2</u>	<b>-0.8</b>	<b>-0.6</b>	<b>-0.8</b>	<u>+0.7</u>	<u>+1.8</u>	<u>+1.7</u>
25	<u>+0.2</u>	<b>-1.0</b>	<b>-1.4</b>	<b>-1.1</b>	<b>-1.6</b>	<b>-1.4</b>	<u>+1.1</u>	<u>+0.3</u>	<u>+0.6</u>
50	<b>-2.1</b>	<b>-3.5</b>	<b>-3.9</b>	<b>-1.9</b>	<b>-1.1</b>	<b>-6.7</b>	<u>+0.9</u>	<u>+0.8</u>	<u>+2.9</u>
100	<b>-4.0</b>	<b>-2.4</b>	<b>-4.6</b>	<b>-4.7</b>	<u>+1.6</u>	<u>+0.9</u>	<u>+2.8</u>	<u>+4.3</u>	<u>+5.6</u>

(b)  $\log(D)$  weighting

Return period / Duration	5-min	10-min	15-min	30-min	60-min	2-hr	6-hr	12-hr	24-hr
2	<u>+0.3</u>	<b>-0.3</b>	<b>-0.1</b>	0	<b>-0.3</b>	<b>-0.3</b>	<u>+0.2</u>	<u>+1.3</u>	<u>+2.9</u>
5	<u>+0.2</u>	<u>+0.2</u>	<u>+0.3</u>	<b>-0.7</b>	<b>-0.6</b>	<b>-0.7</b>	<u>+0.1</u>	<b>-0.2</b>	<u>+1.1</u>
10	0	<b>-0.1</b>	<u>+0.1</u>	<b>-0.9</b>	<b>-0.8</b>	<b>-1.0</b>	<b>-0.1</b>	<u>+1.0</u>	<u>+0.9</u>
25	<u>+0.1</u>	<b>-1.0</b>	<b>-1.6</b>	<b>-1.3</b>	<b>-1.5</b>	<b>-1.6</b>	<u>+0.3</u>	<b>-0.8</b>	<b>-0.8</b>
50	<b>-2.1</b>	<b>-3.6</b>	<b>-4.1</b>	<b>-2.4</b>	<b>-1.4</b>	<b>-7.0</b>	<u>+0.1</u>	<b>-0.8</b>	<u>+0.7</u>
100	<b>-3.3</b>	<b>-2.5</b>	<b>-5.0</b>	<b>-5.6</b>	<u>+0.6</u>	<u>+0.3</u>	<u>+1.6</u>	<u>+1.7</u>	<u>+1.9</u>

Table 2: Summary of quantile regression error ratio  $R_\tau$  stratified by duration  $D$  between at-site ECCC IDF curves and ungauged MCQRNN predictions for all stations. Values  $\geq 0.9$  are shown in bold.

Return period / Duration	5-min	10-min	15-min	30-min	60-min	2-hr	6-hr	12-hr	24-hr
2	<b>1.05</b>	<b>0.97</b>	<b>0.98</b>	<b>0.99</b>	<b>0.99</b>	<b>0.98</b>	<b>0.95</b>	<b>0.94</b>	<b>0.97</b>
5	<b>1.06</b>	<b>0.96</b>	<b>0.97</b>	<b>0.99</b>	<b>0.99</b>	<b>0.98</b>	<b>0.94</b>	<b>0.93</b>	<b>0.95</b>
10	<b>1.05</b>	<b>0.94</b>	<b>0.95</b>	<b>0.99</b>	<b>0.99</b>	<b>0.97</b>	<b>0.92</b>	<b>0.90</b>	<b>0.93</b>
25	<b>1.03</b>	<b>0.91</b>	<b>0.91</b>	<b>0.99</b>	<b>0.98</b>	<b>0.97</b>	0.89	0.85	0.88
50	<b>1.02</b>	<b>0.90</b>	0.89	<b>0.95</b>	<b>0.97</b>	<b>0.95</b>	0.86	0.79	0.84
100	<b>0.99</b>	0.87	0.85	0.89	<b>0.94</b>	<b>0.91</b>	0.78	0.74	0.78